

Irrigation impact on boundary layer and precipitation characteristics in Weather Research and Forecasting model simulations during LIAISE-2021

Mireia Udina¹ | Eric Peinó¹ | Francesc Polls¹ | Jordi Mercader² | Iciar Guerrero² | Arianna Valmassoi³ | Alexandre Paci⁴ | Joan Bech^{1,5}

¹Department of Applied Physics–Meteorology, University of Barcelona, Barcelona, Spain

²Meteorological Service of Catalonia, Department of Climate Action, Food and Rural Agenda, Generalitat de Catalunya, Barcelona, Spain

³German Weather Service, Offenbach, Germany

⁴Météo-France/CNRS, Toulouse, France

⁵Institute of Water Research (IdRA), University of Barcelona, Barcelona, Spain

Correspondence

Mireia Udina, Department of Applied Physics–Meteorology, University of Barcelona, Barcelona, 08028, Spain.
 Email: mudina@meteo.ub.edu

Funding information

MCIN/AEI/10.13039/501100011033,
 Grant/Award Numbers:
 PID2021-124253OB-I00(ARTEMIS),
 RTI2018-098693-B-C32(WISE-PreP);
 Water Research Institute (IdRA) of the
 University of Barcelona

Abstract

The Land Surface Interactions with the Atmosphere over the Iberian Semi-arid Environment (LIAISE) campaign examined the impact of anthropization on the water cycle in terms of land–atmosphere–hydrology interactions. The objective of this study is to assess the effects of irrigation on the atmosphere and on precipitation in Weather Research and Forecasting model simulations during the LIAISE special observation period in July 2021. Comparisons between simulations and observations show better verification scores for air temperature, humidity, and wind speed and direction when the model included the irrigation parametrization, improving the model warm and dry bias at 2 m over irrigated areas. Other changes found are the weakening of the sea breeze circulation and a more realistic surface energy partitioning representation. The boundary-layer height is lowered in the vicinity of irrigated areas, causing a decrease in the lifting condensation level and the level of free convection, which induce increases in convective available potential energy and convective inhibition. Precipitation differences between simulations become relevant for smaller areas, close to the irrigated land. When convection is parametrized, simulations including irrigation tend to produce a decrease in rainfall (negative feedback), whereas convection-permitting simulations produce an increase (positive feedback), although the latter underestimates substantially the observed precipitation field. In addition, irrigation activation decreases the areas exceeding moderate hourly precipitation intensities in all simulations. There is a local impact of irrigated land on model-resolved precipitation accumulations and intensities, although including the irrigation parametrization did not improve the representation of the observed precipitation field, as probably the precipitation systems during the LIAISE special observation period in July 2021 were mostly driven by larger scale perturbations or mesoscale systems, more than by local processes. Results reported here not only contribute to enhance our understanding of irrigation effects upon precipitation but also demonstrate the need to include irrigation parametrizations in numerical forecasts to overcome the biases found.

KEY WORDS

convection parametrization, irrigation, precipitation, WRF

1 | INTRODUCTION

Anthropogenic land-use and land-cover changes can modify substantially the physical characteristics of the environment and impact significantly weather and climate (Mahmood *et al.*, 2014; Pielke *et al.*, 2011), as recognized in the Coupled Model Intercomparison Projects (CMIP) in support to the Intergovernmental Panel on Climate Change. In particular, adding water to the soil through irrigation has a direct impact on modifying the energy balance, increasing soil moisture, and altering the land-surface properties. These changes have relevant effects on the thermodynamic properties of the low-level atmosphere (Moiwo & Tao, 2015; Pielke *et al.*, 2016). Irrigation leads to modifications in the surface energy budget partitioning, increasing latent heat fluxes (LEs) at the expense of sensible heat fluxes (SHs), increasing evapotranspiration from the soil and transpiration of plants (Zaveri & Lobell, 2019), producing a cooling near the surface air (Brooke *et al.*, 2023; Lawston *et al.*, 2020; McDermid *et al.*, 2023) and an enhancement of water vapor content in the lower atmosphere (de Vrese & Hagemann, 2018), among others. These mechanisms can modify local and regional circulations, cloud formation, boundary-layer structure, and subsequent precipitation processes (Phillips *et al.*, 2022; Taylor *et al.*, 2012; Van Baelen *et al.*, 2011; Yang *et al.*, 2023).

Land-surface models typically include evapotranspiration, but until very recently the specific parametrization of irrigation has not been considered in operational models—for instance, see Valmassoi *et al.* (2020a). Although in semi-arid and arid conditions it was found that land-surface parameters such as soil moisture seem as important as atmospheric conditions, the large-scale factors can highly determine the occurrence of convection (Maurer *et al.*, 2015). In addition, modeling studies have determined that a fraction of irrigation can have significant local and downstream atmospheric impacts (Lawston-Parker *et al.*, 2023; McDermid *et al.*, 2023).

Irrigation in land-surface models needs to be included in numerical weather simulations and future climate projections in order to correctly represent its effects on the atmosphere (Lavers *et al.*, 2022; Qian *et al.*, 2020; Valmassoi & Keller, 2022), particularly surface temperature cooling (Kueppers *et al.*, 2007; Sacks *et al.*, 2009) and mitigation of heat extremes (Thiery *et al.*, 2017). Many studies have dedicated efforts to examine the effects of irrigation in South Asia and India (Barton *et al.*, 2020, 2023; Douglas *et al.*, 2006; Lee *et al.*, 2009; Saeed *et al.*, 2009), north China (Fan *et al.*, 2023), West Africa (Semeena *et al.*, 2023), the western United States (Pei *et al.*, 2016; Yang *et al.*, 2017), the central United States (Huber *et al.*, 2014; Qian *et al.*, 2020; Rappin *et al.*, 2021), or

southern Europe (Valmassoi *et al.*, 2020b) by including surface irrigation model parametrizations (Valmassoi *et al.*, 2020a). Specifically in the Weather Research and Forecasting (WRF) model, different approaches have been used to include irrigation effects depending on threshold and timing definition (Valmassoi & Keller, 2022), none of them changing the main land parameters: the prescribed irrigation water amount (Valmassoi *et al.*, 2020a, 2020b) and the soil-driven irrigation water amount (Pei *et al.*, 2016; Whitesel *et al.*, 2024; Yang *et al.*, 2017, 2019). Recent parametrizations also included the role of vegetation in the altered land-atmosphere interaction due to irrigation (Asmus *et al.*, 2023).

Analysis of feedbacks between soil moisture and precipitation have revealed positive feedbacks using observations (DeAngelis *et al.*, 2010). However, other studies based on remote-sensing data indicated that the sign of the soil moisture–precipitation feedback may vary depending on the spatial and temporal scales considered (Guillod *et al.*, 2015). Tuttle and Salvucci (2016) highlighted the dependence of the feedback soil moisture–precipitation on the regional aridity of the soil, and Taylor *et al.* (2012) showed enhanced afternoon moist convection driven by increased SH over drier soils. In India, modelling results show that irrigation did not change rainfall over the irrigated area but downwind due to orographic enhancement mechanisms (Fletcher *et al.*, 2022; Turner *et al.*, 2020). In the Great Plains in Nebraska, United States, a modelling case study revealed that precipitation declined with increased irrigation (Whitesel *et al.*, 2024).

Other studies have raised the influence of the convective parametrization activation in the sign of feedbacks (Taylor *et al.*, 2013), depending on the spatial scale as well. Indeed, model grid spacings of a few kilometres (below 10 km) fall within the grey zone for cumulus convection parametrizations, where these parametrization assumptions may be invalid but at the same time the grid may be too coarse to explicitly resolve vertical movements. At 3 or 4 km grid spacing there are a variety of studies either using explicit convection, the so-called convection-permitting simulations (Prein *et al.*, 2015), or still activating cumulus parametrizations, the so-called convection-parametrized simulations (Jeworrek *et al.*, 2021). However, there are no clear criteria for the best option for precipitation systems representation. This horizontal grid spacing may often be insufficient to represent small convective showers or individual convective cells (Jeworrek *et al.*, 2021) but it can explicitly resolve extreme convection events (Horvath *et al.*, 2018; Mastrangelo *et al.*, 2011; Qian *et al.*, 2020). On the other hand, the so-called adjusted scale-aware convection parametrization schemes can improve the representation of deep convection in the grey zone (Jeworrek

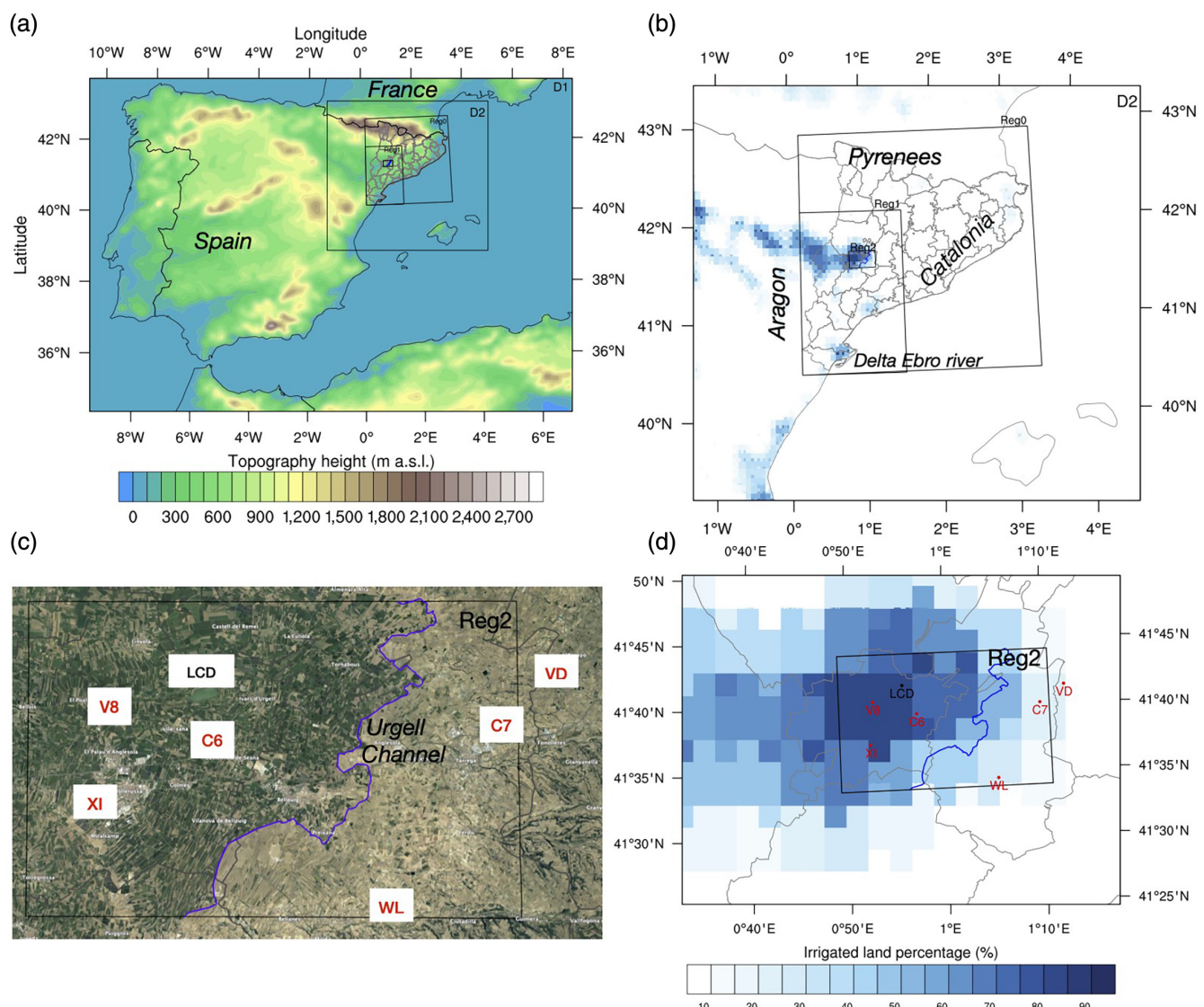


FIGURE 1 Area of study. (a) Topography of the model domains D1 and D2 (9 km and 3 km grid sizes respectively), and limits of Region 0 (Reg0), Region 1 (Reg1), and Region 2 (Reg2). (b) Irrigated land percentage in the Weather Research and Forecasting (WRF) model included in domain D2 and boundaries of Region 0, Region 1, and Region 2. (c) Google Earth image of Region 2 that includes the Urgell Channel (blue contour) and the locations of the ground automatic weather stations Mollerussa (XI), Castellnou de Seana (C6), El Poal (V8), Tàrrega (C7), El Canós (VD), and Sant Martí de Riucorb (WL) and La Cendrosa (LCD) tower. (d) Detail of the irrigated land percentage in the WRF model included in Region 2 and the same elements represented in (c).

et al., 2019; Steeneveld & Peerlings, 2020), with a better skill for smaller grid spacings.

Recent field campaigns have been dedicated to study the impact of irrigated land cover on land-atmosphere interactions and weather: the Great Plains Irrigation Experiment campaign (Rappin et al., 2021) in the Great Plains (Nebraska, United States) during spring and summer 2018 and the Land Surface Interactions with the Atmosphere over the Iberian Semi-Arid Environment (LIAISE) campaign (Boone et al., 2021) in summer 2021. The LIAISE initiative aimed to improve our understanding of key natural and anthropogenic land processes and

the subsequent feedbacks with the boundary layer and the Mediterranean basin hydrological cycle. An extensive deployment of instrumentation was undertaken in the area of the eastern Ebro basin (northeast Iberian Peninsula; see Figure 1) in summer 2021, including specially equipped aircraft, ground-based atmospheric profilers, and an enhanced network of ground stations and sensors (Boone et al., 2021). The most intensive observational stage of the LIAISE campaign was the so-called second special observation period (SOP) that took place during July 15–31, 2021, the period analysed in this study. The LIAISE domain is a region where intense agricultural

activity has altered the land use and land cover, including an irrigated area in the western part and a rain-fed surface in the eastern part (Figure 1) of the eastern Ebro basin. This anthropogenized land-cover heterogeneity in a semi-arid Mediterranean region makes it an area of special interest of study according to the CMIP projections including the land-use and land-cover changes implemented in CMIP6 (Eyring *et al.*, 2016).

Our study aim is to explore the irrigation impact on precipitation processes using the WRF model during the LIAISE SOP with the following research questions:

1. What is the impact of including irrigation in WRF simulations in surface and boundary-layer variables?
2. How do the model simulations compare against observations for ground stations and precipitation estimates that combine rain-gauges and weather radar?
3. Which is the sign of irrigation feedback on precipitation in model simulations depending on the treatment of convection?

The rest of the article is organised as follows. Section 2 describes the area of study, the WRF numerical simulation configuration, the observational data used, and the verification metrics. Section 3 presents the model verification, including temperature, humidity, and wind from surface stations, precipitation estimates from weather radar, and flux measurements from a tower. Section 4 explains the impact of irrigation parametrization on the temporal and spatial distribution of the main meteorological variables, and a discussion and conclusions are given in Section 5.

2 | METHODS

2.1 | Area of study

The area of study is the eastern Ebro basin located in the northeast of the Iberian Peninsula (Figure 1a), a relatively flat area devoted to agriculture activity that includes a large extension of irrigated land close to another rain-fed area (Dari *et al.*, 2023), separated by the Urgell Channel (Figure 1c). The climate of the study region is semi-arid, Bsk according to the Köppen climatic classification. Locally, it is characterized by an extreme surface heterogeneity with a sharp contrast between the irrigated and the rain-fed areas, reaching substantial differences in horizontal distances of just 10 km (Mangan *et al.*, 2023a). The shape, orientation, and extension of the basin have a great influence on the synoptic and mesoscale circulations in the northeast of the Iberian Peninsula, as northern and western surface flows are often channelized

following the Ebro Valley orientation (Bech *et al.*, 2015; Gonzalez *et al.*, 2018; Lee *et al.*, 2017). In addition, the Mediterranean Sea is located approximately 70 km to the southeast, which induces sea-breeze circulations during the warm season in the absence of strong synoptic forcing.

Three different regions are delimited to perform the analysis of the model results: Region 0, Region 1, and Region 2, covering different extents, from larger to smaller areas (Figure 1a,b). Region 0 corresponds to the largest area, including Catalonia, where weather radar quantitative precipitation estimates (QPEs) are available. Region 1 covers the southeast Ebro basin and the southeast of Catalonia. Region 2 (Figure 1c), a $30 \times 21 \text{ km}^2$ rectangle, is the smallest region and includes the Urgell Channel (blue solid line in Figure 1c), an artificial water channel that delimits the irrigated area (west) and the non-irrigated area (east).

2.2 | Data

2.2.1 | WRF simulations

The numerical simulations are performed using the WRF model (Skamarock *et al.*, 2021) in the Advanced Research WRF (ARW) version 4.3. We use two one-way nested domains of 9 km (domain D1) and 3 km (domain D2) horizontal grid resolutions, with 166×115 grid cells in D1 and 166×154 cells in D2, both centred at 39.36° N , 1.1766° W . In the vertical, the 31 levels defined by the default configuration in WRF-ARW (Wang *et al.*, 2007) are considered, based on previous studies in the area (Farnell *et al.*, 2022; Mercader *et al.*, 2010; Udina *et al.*, 2017), and to keep a reasonable computational cost according to several sensitivity tests. Model top is defined at 100 hPa. The simulation is continuously run from July 1 to 31, 2021, but the first 15 days are taken as irrigated spin-up. Therefore, only the last 17 days of July are analysed; that is, the period from July 15 to 31, 2021, corresponding to the second SOP of the LIAISE campaign (Boone *et al.*, 2021; Mangan *et al.*, 2023a). The model configuration and physics options used in this study are summarized in Table 1. Note that cumulus convection parametrization is not activated for simulations presented in Section 4.3.

The model utilizes initial and boundary conditions from European Centre of Medium-range Weather Forecasts Reanalysis v.5 (ERA5) (Hersbach *et al.*, 2020; Copernicus Climate Change Service (C3S), 2017), with horizontal resolution of 0.25° , 38 vertical levels, and temporal resolution of 1 hr. Analysis nudging is applied every 6 hr as, after several sensitivity tests, nudging was found to be necessary for a more realistic simulation of rainfall. In the

TABLE 1 Weather Research and Forecasting (WRF) model configuration and physics parametrizations.

WRF scheme	Option	Reference
Long-wave radiation	Rapid Radiative Transfer Model	Mlawer <i>et al.</i> (1997)
Short-wave radiation	Dudhia scheme	Dudhia (1989)
Land-surface	Unified Noah land-surface model	Tewari <i>et al.</i> (2004)
Surface layer	Revised Mesoscale Model (MM5) Monin–Obukhov scheme	Jiménez <i>et al.</i> (2012)
Boundary layer	Yonsei University scheme	Hong <i>et al.</i> (2006)
Microphysics	WRF Single Moment 5-class scheme	Hong <i>et al.</i> (2004)
Cumulus convection	Kain–Fritsch (new Eta) scheme (deactivated in Section 4.3)	Kain (2004)

planetary boundary layer (PBL), nudging is only applied in wind components, not for temperature and humidity. Sensitivity tests demonstrate a better agreement with surface stations for simulated wind speed when applying nudging in wind components within the PBL. One-way nested domains preserve the boundary conditions from ERA5, maintaining the one-third grid resolution ratio between domains, as recommended for WRF simulations (Skamarock *et al.*, 2021).

The irrigated-area map used in the simulations is sourced from the Food and Agriculture Organisation (FAO) database (Siebert *et al.*, 2013) included in the WRF WPS v4 Geographical Static Data, calculated as a percentage of irrigated area in each grid. In the northeastern part of the Iberian Peninsula, irrigated fields are concentrated in the Ebro basin (see Figure 1b,d), prevailing in an area extending from eastern Aragon and western Catalonia. As can be seen, all grid points in Region 2 are irrigated at a certain percentage, although the highest irrigated land percentages are observed west of the Urgell Channel (Figure 1d). From the three options available in the WRF irrigation parametrization, we have applied the channel system (Valmassoi *et al.*, 2020a; option 1), where the irrigation water is applied directly to the surface, and neglecting interactions with the canopy. As explained in Valmassoi *et al.* (2020a), the channelling option accounts for evaporation from the soil and water at the surface, where the amount of water irrigated is the input for the land-surface model, in this case the Noah land-surface model. The other surface physiographic parameters, such as albedo, leaf area index, or vegetative fraction, were not altered. The amount of irrigated water, scaled to the percentage of irrigated land in each grid (Figure 1d), was set to $2.85 \text{ mm} \cdot \text{day}^{-1}$, a value consistent with recent irrigation estimates derived from satellite observations in the Ebro basin (Dari *et al.*, 2023). This amount represents half of the reference value ($5.7 \text{ mm} \cdot \text{day}^{-1}$) chosen for simulations in the Po Valley in Valmassoi *et al.* (2020b). In our experiments, following the farmers' practices during LIAISE, this irrigation rate is applied every night during

12 hr, from 1800 UTC to 0600 UTC (2000 h to 0800 h local time) (Table 2).

Using the physics parametrizations from Table 1, the main model experiments defined in this study consider a control case (CTL) where no irrigation is added and an irrigated experiment (IRR) where the irrigation parametrization (Valmassoi *et al.*, 2020a) is applied in the area shown in Figure 1b,d. Additional sensitivity model experiments were run deactivating cumulus convection parametrization (convective-permitting simulations), whose results are included in Section 4.3, considering also control (CTL_{cp}) and irrigated (IRR_{cp}) cases (Table 2).

2.2.2 | Observational data

To quantify the model performance we use six ground stations from the Meteorological Service of Catalonia automatic weather station network: Mollerussa (XI), El Poal (V8), and Castellnou de Seana (C6) located in the irrigated area west of Urgell Channel, and Tàrrega (C7), El Canós (VD), and Sant Martí de Riucorb (WL), located in the non-irrigated area east of Urgell Channel (see Figure 1). The stations report air temperature, humidity, wind speed, wind direction, solar radiation, and precipitation every 30 min, although only hourly values are compared against the model output.

The precipitation validation of the control and irrigated WRF simulations was done using the Hydrometeorological Integrated Forecasting Tool (hereafter EHIMI) system (Bech *et al.*, 2005; Rigo *et al.*, 2021) as a reference. This product, developed by the Applied Research Centre in Hydrometeorology of the Polytechnic University of Catalonia and implemented operationally in collaboration with Meteorological Service of Catalonia, combines information from the accumulated radar precipitation and the rain-gauge network in Catalonia to finally provide QPEs at an hourly resolution and at 1 km spatial resolution. The weather radar coverage over Region 1 and Region 2 is good, but over the northern Pyrenees (north part of Region 0)

TABLE 2 Weather Research and Forecasting model simulations including control (CTL) and irrigated (IRR) cases for cumulus convection parametrized experiments (first two rows) and CTL and IRR convection-permitting (cp) experiments (last two rows).

Simulation	Irrigation	Cumulus convection	Amount (mm·day ⁻¹)	Start–final hour
CTL	None	Parametrized	0.00	None
IRR	Yes	Parametrized	2.85	1800–0600 UTC
CTL _{cp}	None	Explicit	0.00	None
IRR _{cp}	Yes	Explicit	2.85	1800–0600 UTC

TABLE 3 Continuous and categorical metrics used to evaluate automatic weather stations and Hydrometeorological Integrated Forecasting Tool estimates against Weather Research and Forecasting control (CTL) and irrigated (IRR) model simulations.

Metric	Formula	Perfect score
<i>Continuous metric</i>		
Mean bias (MB)	$MB = \frac{1}{n} \sum_{i=1}^n (M_i - O_i)$	0
Relative bias (Rbias)	$Rbias = \frac{\sum_{i=1}^n (M_i - O_i)}{\sum_{i=1}^n O_i} \times 100$	0
Root-mean-square error (RMSE)	$RMSE = \sqrt{\frac{1}{n} \sum_{i=1}^n (M_i - O_i)^2}$	0
Mean absolute error (MAE)	$MAE = \frac{\sum_{i=1}^n M_i - O_i }{n}$	0
<i>Categorical metric</i>		
Probability of detection (POD)	$POD = \frac{\text{Hits}}{\text{Hits+Misses}}$	1
False-alarm rate (POFD)	$POFD = \frac{\text{False alarms}}{\text{False alarms+Correct negatives}}$	0
Hansen and Kuipers (HK)	$HK = POD - POFD$	1

Note: M_i and O_i correspond to the model and the observation values respectively for each time step i and for the total number of time steps n .

mountain beam blockage limits the quality—see Trápero *et al.* (2009) for more details.

On the other hand, additional measurements from the 50 m tower located at La Cendrosa (Canut, 2022) are used to compare energy and momentum fluxes near the surface. More specifically, measurements of the surface SH, surface LE, friction velocity at 3 m level, and soil temperature at 5 cm are explored.

2.3 | Verification metrics

The numerical experiment verification has been conducted using continuous and categorical scores. For continuous variables, mean bias (MB), root-mean-square error (RMSE) and mean absolute error (MAE) have been considered for WRF model simulations compared against the automatic weather stations and against radar QPEs (see Table 3). To compare wind speed at 10 m above ground level obtained from the model with the wind speed at 2 m above ground level measured at some Meteorological Service of Catalonia automatic weather stations (XI, V8, VD, WL), a wind profile power-law relationship is applied to observations, considering an exponent of 0.25, for an urban, neutral case (Irwin, 1979).

The ability of WRF to correctly detect precipitation events in comparison with EHIMI estimates is also explored using categorical scores based on a standard contingency table (see Appendix A, Table A.1) including the probability of detection (POD), false-alarm rate (POFD), also known as probability of false detection, and a combined index of the last two, the Hansen and Kuipers (HK) categorical score (Jolliffe & Stephenson, 2012; Trápero *et al.*, 2013) (Table 3). The HK statistic measures the ability of the forecasting system to separate observed “yes” and “no” cases. It was calculated from a 2 × 2 contingency table that classifies as events exceeding selected intensity thresholds (0.1, 1, 2, 5, 10, and 15 mm·day⁻¹).

The upscaling method from Zepeda-Arce *et al.* (2000) was used as a fuzzy verification technique on daily precipitation accumulations in Regions 0 and 2. As described in Ebert (2008), unlike traditional scores, the fuzzy verification by “neighbourhood observation minus neighbourhood forecast” responds to a point of view in which observations are scaled to represent the scales resolved by the model, typically several grid lengths. As the study datasets are affected by having different spatial resolutions, in WRF (3 km) and EHIMI (1 km), both products were rescaled to common resolutions of 3, 6, 9, 15, and 27 km using the distance-weighted mean (Li *et al.*, 2019; Van Osnabrugge

et al., 2017) as the regrid scheme. The new gridded data enabled a pixel-to-pixel comparison between the WRF model experiments, CTL and IRR, and the EHIMI estimates of precipitation.

2.4 | Other methods

To complement the analysis described herein, statistical tests were performed. In particular, the statistical significance of differences in precipitation between the control and the irrigated simulations is tested using the Wilcoxon signed-rank test (Woolson, 2007), a non-parametric test suitable for paired samples with the same distribution.

3 | VERIFICATION

3.1 | Surface stations

Metrics of temperature simulations are improved in all six surface stations when including the irrigation parametrization (Table 4). MB is lowered from 1.14 K in CTL to 0.82 K in IRR (−28%), whereas RMSE is lowered from 1.92 K in CTL to 1.76 K IRR (−8%). Errors are even more strongly reduced for daily maximum temperatures, reaching a 19% reduction in RMSE when including irrigation in simulations. Figure 2 illustrates the automatic weather station individual errors for temperature, showing a greater reduction in errors for stations located in the irrigated area (underlined XI, C6, and V8) than the ones located in the dry area (C7, VD, WL). A warm bias exists in all stations for both simulations for the 2 m

temperature (Figure 2a), although the 2 m maximum temperatures in some stations have a cold bias when including the irrigation parametrization (Figure 2b). In contrast, minimum temperatures in IRR are not improved, so that RMSE and MAE errors increase by 17% and 23% respectively as a consequence of a too low soil temperature.

Regarding specific humidity at 2 m, MB is significantly reduced when including irrigation (from −0.44 in CTL to 0.13 in IRR), and RMSE and MAE are also improved by around −18% and −20% respectively. Looking at individual automatic weather station errors, we can see that the specific humidity is underestimated (dry bias) in CTL simulations in stations located in the irrigated area (XI, C6, and V8) whereas it is reversed and fairly well adjusted when including irrigation parametrization (Figure 2c). Similar results are obtained for wind speed, with an improvement of metrics in IRR simulations, with a reduction of the MB, RMSE, and MAE of −18%, −8%, and −10% respectively. Wind speed decreases at all stations from CTL to IRR simulations (Figure 2d), meaning that the irrigation impacts the momentum exchange by decelerating the flow. Wind direction is improved as well in IRR simulation, with slightly reduced MB, RMSE, and MAE.

3.2 | Precipitation

Figure 3 illustrates the accumulated precipitation in the 17-day period from EHIMI estimates (Figure 3a), from the CTL simulation (Figure 3b), and from the IRR simulation (Figure 3c) in Region 0. In general, the model simulations underestimate precipitation quantities on the

TABLE 4 Continuous verification metrics for Weather Research and Forecasting control (CTL) and irrigated (IRR) simulations compared with the six Meteorological Service of Catalonia automatic weather stations.

Variable (units)	Simulation	MB	RMSE	MAE
2 m temperature (K)	CTL	1.14	1.92	1.50
	IRR	0.82	1.76	1.30
2 m maximum temperature (K)	CTL	0.97	1.42	1.21
	IRR	−0.24	0.90	0.74
2 m minimum temperature (K)	CTL	1.29	2.02	1.62
	IRR	1.79	2.36	2.00
2 m specific humidity ($\text{g}\cdot\text{kg}^{-1}$)	CTL	−0.44	1.90	1.48
	IRR	0.13	1.57	1.19
10 m wind speed ($\text{m}\cdot\text{s}^{-1}$)	CTL	1.14	1.93	1.62
	IRR	0.93	1.78	1.46
10 m wind direction (deg)	CTL	−21.70	50.58	50.58
	IRR	−17.14	48.19	48.19

Abbreviations: MAE, mean absolute error; MB, mean bias; RMSE, root-mean-square error.

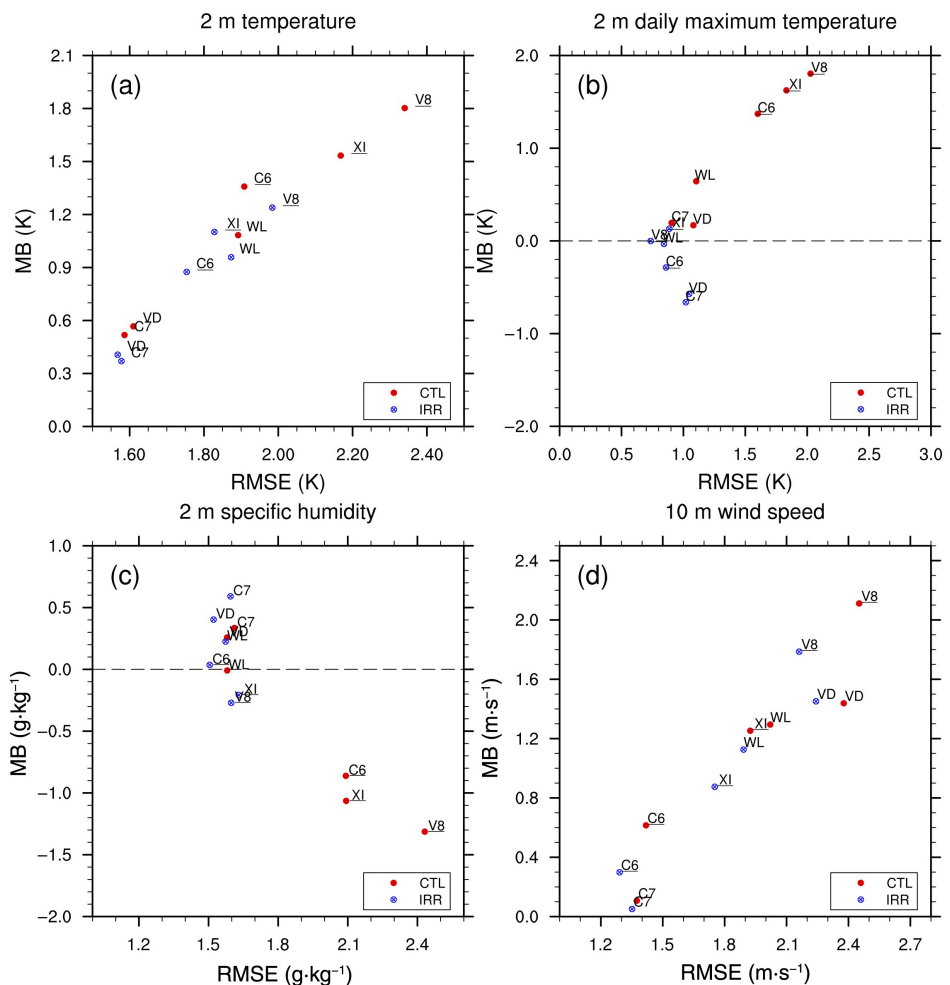


FIGURE 2 Mean bias (MB) and root-mean-square error (RMSE) for (a) 2 m temperature, (b) 2 m daily maximum temperature, (c) 2 m specific humidity, and (d) 10 m wind speed in control (CTL) and irrigated (IRR) simulations at six Meteorological Service of Catalonia automatic weather stations. Stations in the west irrigated area (Castellnou de Seana, C6; Mollerussa, XI; El Poal, V8) are underlined, whereas stations in the non-irrigated area (Tàrrrega, C7; Canós, VD; Sant Martí de Riucorb, WL) are labelled in normal text.

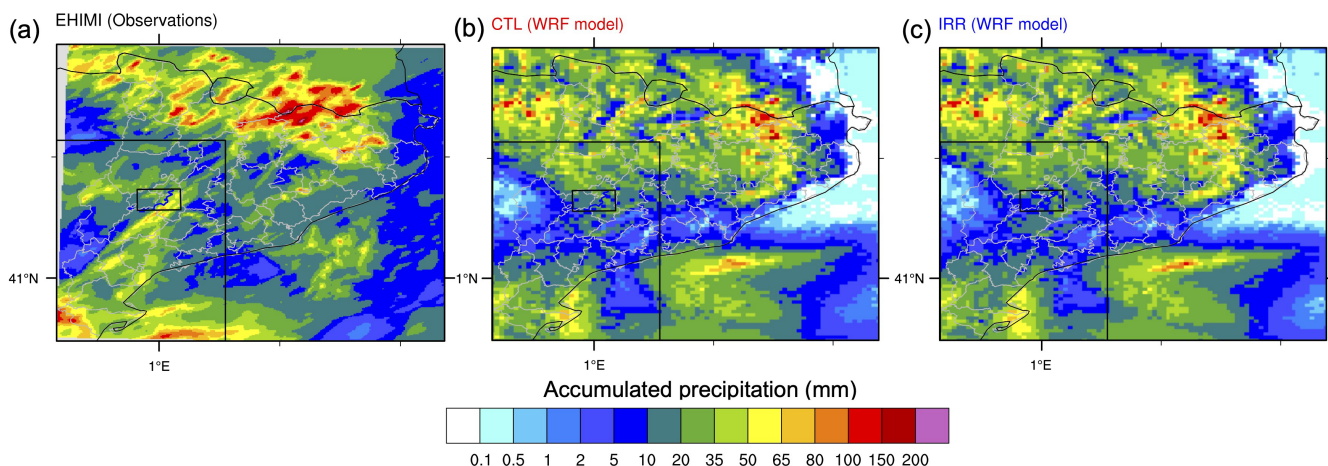


FIGURE 3 Accumulated precipitation for the whole period (July 15–31, 2021) in Region 0 for (a) quantitative precipitation estimates (QPEs) of the Hydrometeorological Integrated Forecasting Tool (EHIMI) corresponding to observations, (b) Weather Research and Forecasting (WRF) control simulation (CTL), and (c) WRF irrigated simulation (IRR). Black boxes on the left indicate limits of Region 1 and inner Region 2. Owing to the geographical domain of the QPEs of the EHIMI products, areas with missing values are shown in grey.

northeast coast and in the mountainous Pyrenean area, whereas a slightly overestimation occurs over the sea, in front of the coast. According to EHIMI, precipitation in Region 0 occurred during 11 days (out of the

17 days studied), with the most important amounts falling on July 20, 26, 30, and 31, whereas precipitation in Region 2 was present only during these former 4 days (see Appendix C).

TABLE 5 Continuous statistics for precipitation calculated for the Weather Research and Forecasting control (CTL) and irrigated (IRR) simulations in the three regions in comparison with the Hydrometeorological Integrated Forecasting Tool (EHIMI) product.

Region	Simulation	MB (mm·day ⁻¹)	Rbias (%)	RMSE (mm·day ⁻¹)	MAE (mm·day ⁻¹)
Region 0	EHIMI vs. CTL	-0.31	-21.0	7.19	2.19
	EHIMI vs. IRR	-0.31	-20.7	7.19	2.18
Region 1	EHIMI vs. CTL	-0.31	-21.8	4.60	1.46
	EHIMI vs. IRR	-0.34	-23.6	4.52	1.43
Region 2	EHIMI vs. CTL	-1.02	-54.4	4.96	1.45
	EHIMI vs. IRR	-1.17	-62.0	5.10	1.45

Abbreviations: MAE, mean absolute error; MB, mean bias; Rbias, relative bias; RMSE, root-mean-square error.

The comparison of CTL and IRR simulations against QPE from EHIMI is shown using continuous statistics (Table 5) and categorical statistics (Figure 4), for daily accumulated precipitation. There is a general underestimation of the simulated daily accumulated precipitation for all the regions considered. Biases and relative errors increase as the regions become smaller (Table 5). For the large Region 0 there are hardly any differences between CTL and IRR simulations, but they become more relevant for smaller areas. For instance, in Region 2 precipitation biases and errors in CTL simulation are slightly smaller than in IRR simulation, which highlights a better, although still poor, performance of CTL simulation in terms of precipitation.

The categorical statistics are shown in Figure 4 for Region 0 and Region 2 and for the two simulations CTL and IRR, splitting the results among five different spatial scales and six different daily precipitation intensity thresholds. As expected, for the large Region 0 the highest POD (also highest HK) is obtained for small precipitation thresholds and tends to increase as the spatial scale increases. In Region 2, large spatial scales of 9, 15, and 27 km seem to be the best to capture events of precipitation intensity thresholds above 5 mm·day⁻¹. Although in Region 0 there are almost no differences between CTL and IRR for the different intensity thresholds and spatial scales, they are more sizeable in Region 2, where larger POD and HK are obtained in CTL for moderate precipitation intensity thresholds from 5 to 15 mm·day⁻¹. The exception is the case at the 15 km scale for rainfall events above 15 mm·day⁻¹, due to the occurrence of one case where WRF CTL recorded 14.19 mm·day⁻¹ and WRF IRR 15.98 mm·day⁻¹ (still, both values are far away from the 45.35 mm·day⁻¹ estimated by EHIMI). Similar scores between CTL and IRR are obtained for low threshold intensities. Moreover, larger spatial scales help the simulations capture the precipitation events, specially in the IRR simulation. As seen in Table 5, in Region 2, CTL reproduces more daily precipitation, closer to the EHIMI

than IRR, which leads to a higher POD in CTL than in IRR simulations for moderate intensity thresholds.

3.3 | Surface energy and momentum exchange

The surface-atmosphere exchange of energy and mass is explored from tower measurements of fluxes at La Cendrosa, an irrigated site representative of a relatively homogeneous terrain area. SH, LE, soil temperature at 5 cm (T_{soil}), and friction velocity (u_*) are compared with the two simulations, CTL and IRR (Figure 5), revealing a general better adjustment when irrigation is activated.

Energy partitioning is very different between IRR and CTL simulations. In CTL, most of the energy is invested in heat (large SH) and a very small amount in evaporation (low LE), only relevant on specific days after rain occurred at that point according to the model (July 28 and July 31) and the soil contained liquid water (Figure 5a,b). Conversely, in IRR, the energy partition is reversed, and the whole period shows a higher LE than SH, meaning that the energy is consumed in evapotranspiration, which includes evaporation from the soil and plant transpiration (Cuxart & Boone, 2020).

Table 6 shows a summary of statistics comparing simulations with observations. Although statistics such as MB, RMSE, and MAE are highly improved in IRR in comparison with CTL simulations, the SH is still overestimated and LE underestimated in both simulations, with RMSE and MAE slightly larger than in other previous case studies (Whitesel *et al.*, 2024). In terms of fluxes, our model runs at 3 km grid sizes seem to be reproducing regional to landscape scales where the surface fluxes are smoother than at local scales, as reported by Mangan *et al.* (2023a).

Soil temperature is better resolved in IRR when irrigation is included in the simulations, although simulated minimum soil temperatures are generally too low (Figure 5c), as there is a slight overestimation in the downward long-wave flux (not shown). Maximum soil

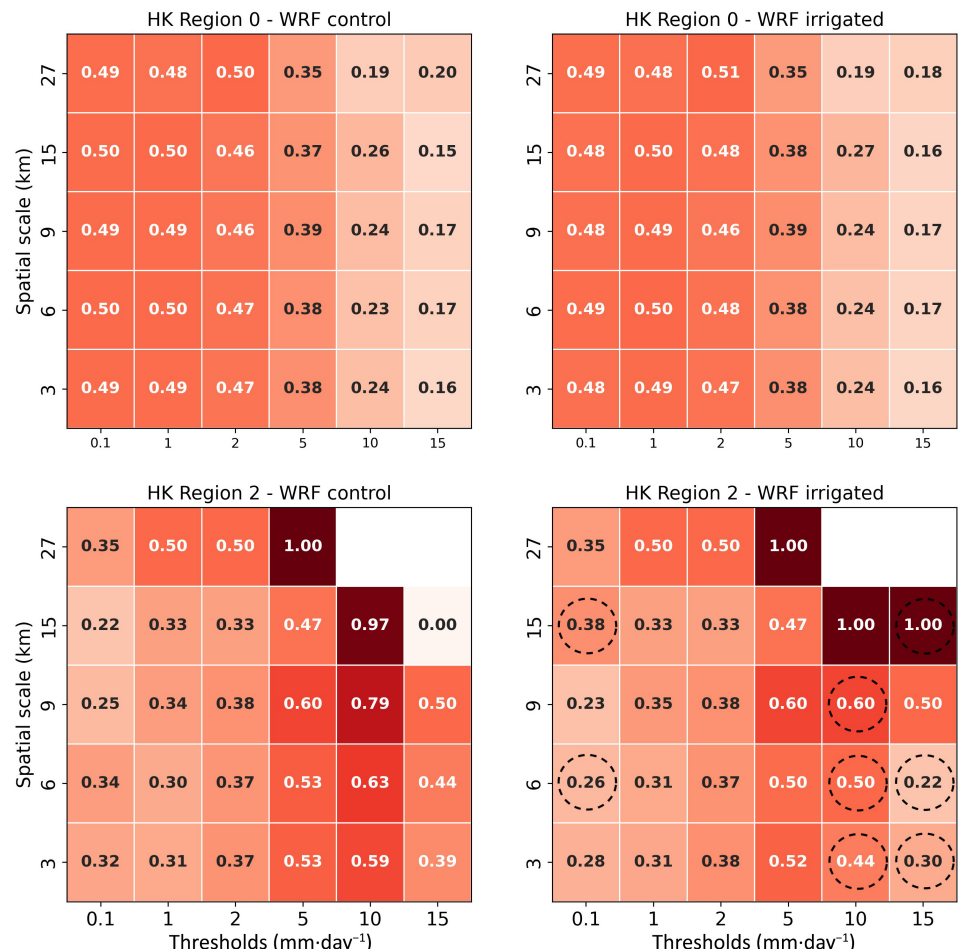


FIGURE 4 Hansen and Kuipers (HK) scores for Region 0 (top row) and Region 2 (bottom row) separating Weather Research and Forecasting (WRF) control simulation (CTL; left column) and WRF irrigated simulation (IRR; right column) simulations against quantitative precipitation estimates, including different spatial resolution aggregations and different intensity thresholds, using convection-parametrized simulations. Highlighted values with a dashed circle indicate differences in HK over 0.05 between the CTL and IRR scores. The darker (lighter) colour indicates good (poor) performance according to the decision model used by the upscaling method.

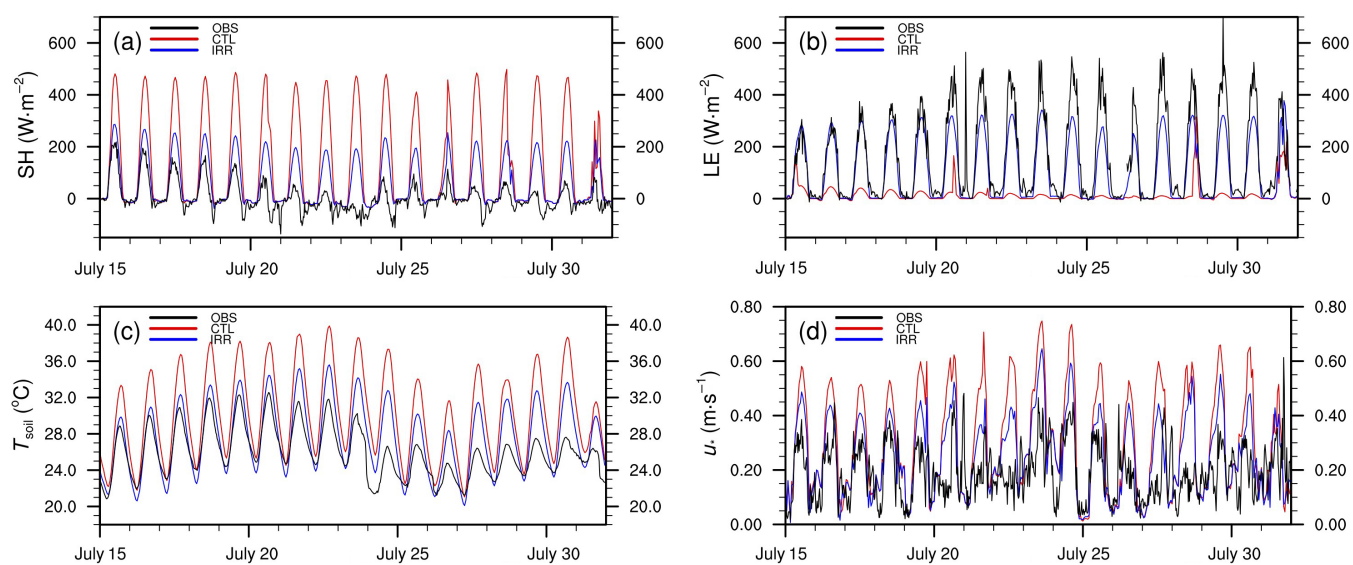


FIGURE 5 Evolution of (a) sensible heat flux (SH), (b) latent heat flux (LE), (c) soil temperature (T_{soil}) at 5 cm, and (d) friction velocity (u_*) from observations (OBS; half-hourly) and from Weather Research and Forecasting control (CTL) and irrigated (IRR) simulations (hourly) at La Cendrosa.

temperatures are well adjusted in the first period of simulation but are still overestimated during the last week, possibly because higher irrigation rates were applied at the site, which were not represented in the model simulations.

The momentum exchange between the surface and the atmosphere is explored using the friction velocity u_* , which also presents significant differences between the two simulations. CTL tends to produce higher friction

TABLE 6 Continuous statistics for sensible heat flux (SH), latent heat flux (LE), soil temperature (T_{soil}) and friction velocity (u_*) calculated for the two Weather Research and Forecasting control (CTL) and irrigated (IRR) simulations in comparison with the tower observations.

Variable (units)	Simulation	MB	RMSE	MAE
SH ($\text{W}\cdot\text{m}^{-2}$)	CTL	131.08	199.26	133.12
	IRR	57.63	85.87	59.50
LE ($\text{W}\cdot\text{m}^{-2}$)	CTL	-141.96	207.06	142.90
	IRR	-47.91	81.00	55.11
T_{soil} (K)	CTL	4.23	5.02	4.23
	IRR	1.56	2.49	1.88
u_* ($\text{m}\cdot\text{s}^{-1}$)	CTL	0.11	0.20	0.16
	IRR	0.06	0.14	0.11

Abbreviations: MAE, mean absolute error; MB, mean bias; RMSE, root-mean-square error.

velocities than IRR does for the 17-day simulations; in turn, this u_* in IRR is closer but often larger than observations from the tower, especially during daytime (Figure 5d). This is in accordance with the stronger resolved wind near the surface described in CTL, as the calculation of u_* from the surface parametrization implies the dependence on wind speed, resulting in flow deceleration when irrigation is activated. As seen in Figure 7, the smaller horizontal temperature gradients reproduced in IRR reduce the wind acceleration due to horizontal pressure gradients (Phillips *et al.*, 2022). In addition, the reduction in the boundary-layer height may lead to a decrease of mixing due to a decrease of downward momentum fluxes at the top of the PBL, which could also lead to a weakening of wind.

4 | IRRIGATION PARAMETRIZATION IMPACT

4.1 | Temperature, moisture, wind, and boundary-layer height

The activation of irrigation parametrization reduces the 2 m air temperature amplitude in both Regions 1 and 2. Higher maximum extreme temperatures in the CTL simulations are identified, mostly in the smaller Region 2, where extreme temperature values ranging from 312 to 315 K are only reached in the CTL simulation, not in the IRR simulation (Figure 6a,e). Differences in 2 m temperature between the simulations reach values around 2 or 3 K in the early afternoon in the areas near the irrigated area (Figure 6i). As expected, 2 m air surface moisture is increased in IRR simulation, shifting from a median value of $10.4 \text{ g}\cdot\text{kg}^{-1}$ in CTL to a median of $10.9 \text{ g}\cdot\text{kg}^{-1}$ in IRR in Region 2 (Figure 6b). The largest differences

between the averaged moisture field at the surface are seen around the irrigated area, where the moisture increases on average between 1.5 and 2 $\text{g}\cdot\text{kg}^{-1}$ (in Figure 6f,j). Wind speed at 10 m is reduced in the IRR simulation, strongly in Region 2 (by a median average of 9%) and more strongly at grid points where more percentage of irrigation is applied (Figure 6k). By contrast, a slight increase in wind speed occurs in IRR north of Region 1. On the other hand, the calculated PBL height (PBLH) is lower in IRR than in CTL (Figure 6d,h), as irrigation inhibits convective thermals that help the mixed layer growing. This difference is clearly seen at grid points where irrigation is applied, when comparing the average PBLH values at 1400 UTC (Figure 6l), reaching significant differences of over 800 m in the boundary-layer depth, with a wide surrounding area of influence in the north of Region 1.

Significant changes in wind speed and wind direction are also seen near areas where irrigation is applied (Figure 6c,g). In the afternoon and late afternoon, the mean wind direction mostly from the southsouthwest in CTL is shifted towards the westsouthwest in the IRR simulation, revealing a modification in the regional circulation due to the irrigation. In fact, a general deceleration of the flow occurs when irrigation is activated, especially during the afternoon (Figure 7a–c). The southern sea breeze or *marinada* (Jiménez *et al.*, 2023) entrance near Region 2 is slowed down in IRR on the specific days when this mesoscale circulation is developed. The delay of the sea breeze entrance in IRR is linked to the inland lower horizontal temperature gradient, as shown in Figure 7d–f. These results are consistent with those found for the larger scale phenomena of the low-level jet in the Great Plains, where irrigation led to a reduction of the low-level jet frequency due to a weakening of temperature gradients (Huber *et al.*, 2014; Phillips *et al.*, 2022; Yang *et al.*, 2020b).

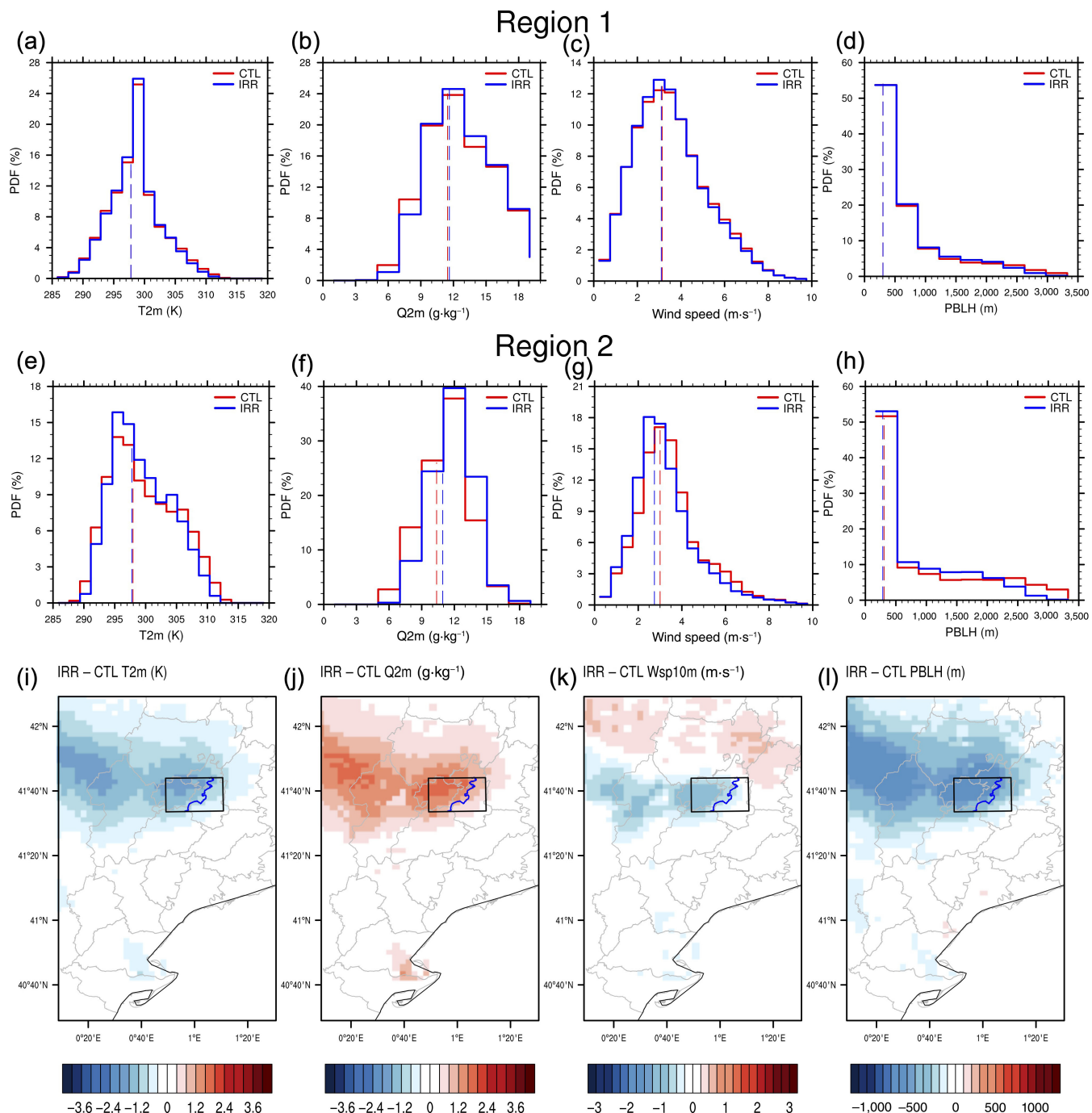


FIGURE 6 (a–h) Model results of (a, e) 2 m air temperature (T2m), (b, f) 2 m air moisture (Q2m), (c, g) 10 m wind speed (Wsp10m), and (d, h) planetary boundary-layer height (PBLH) probability distributions for Weather Research and Forecasting control (CTL) and irrigated (IRR) simulations for grid points included in (a–d) Region 1 and (e–h) Region 2. Red and blue dashed lines respectively indicate the median values of the CTL and IRR simulations. (i)–(l) Model simulations differences (IRR minus CTL) for the averaged fields at 1400 UTC for the period July 15–31 of (i) T2m, (j) Q2m, (k) 10 m wind speed, and (l) PBLH. PDF: probability density function.

4.2 | Precipitation distribution and related parameters

Changes in precipitation accumulation and intensities between the CTL and IRR simulations are analysed

here for the three regions for the 17-day period of July 15–31, 2021. As commented earlier, activation of irrigation parametrization (IRR) leads to very inappreciable changes in accumulated precipitation in the large Region 0 and a slight decrease in Region 1 (−3%) for the whole

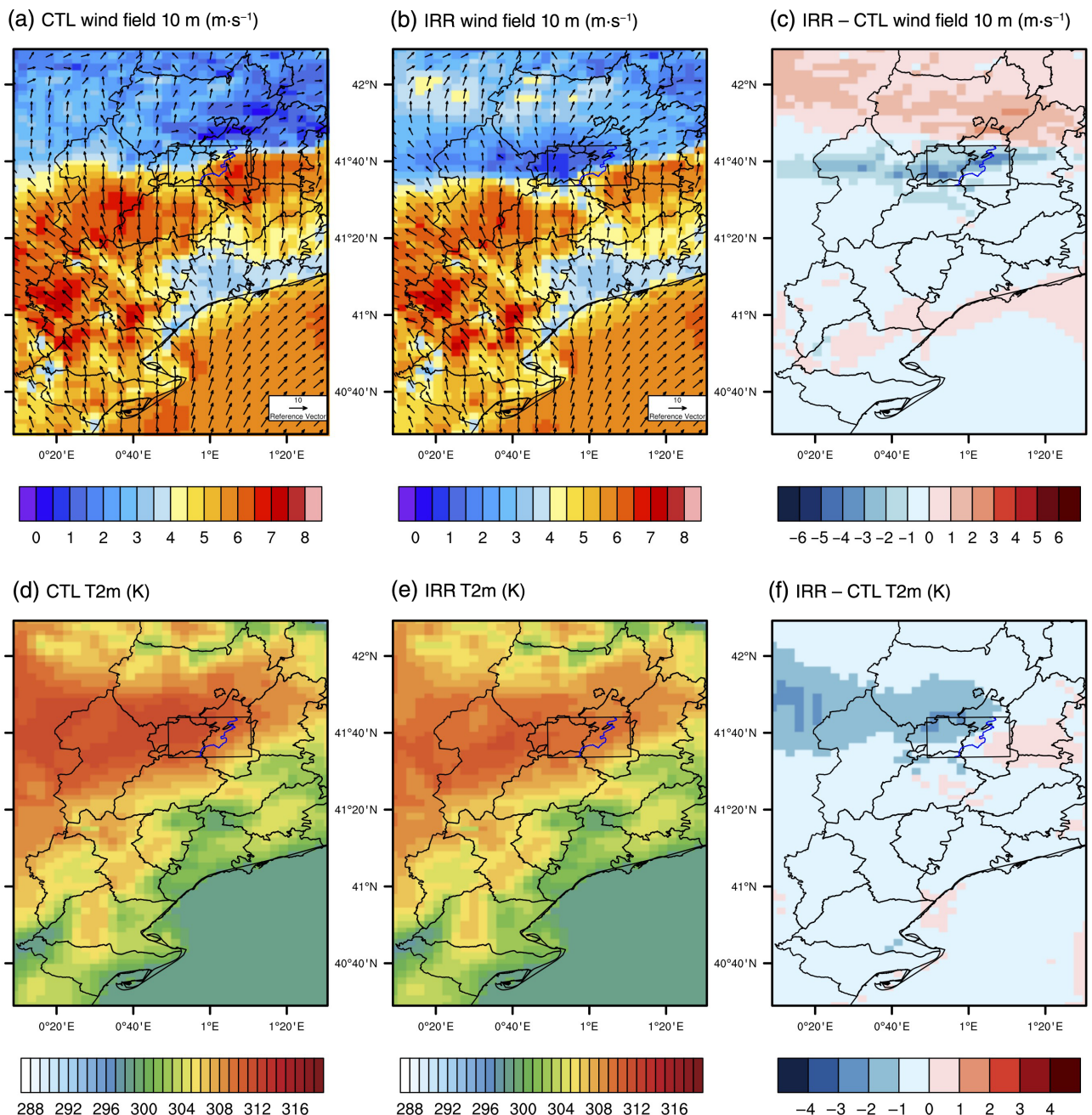


FIGURE 7 (a)–(c) Model results of wind field at 10 m from Weather Research and Forecasting (a) control (CTL) simulation, (b) irrigated (IRR) simulation, and (c) their differences (IRR minus CTL). (d)–(f) Air temperature at 2 m (T2m) from (d) CTL simulation, (e) IRR simulation, and (f) their differences (IRR minus CTL). All plots are for July 21, 2021, at 1500 UTC.

period considering all grid points of the domains. A more important reduction in precipitation is reproduced in Region 2 (-15%) when irrigation is activated, where, in addition, all grid points in this region are irrigated at some percentage (Table 7). In terms of precipitation intensities, IRR produces a lower number of grid points where precipitation is above 3 or $5 \text{ mm}\cdot\text{hr}^{-1}$ threshold in both Region 1 and Region 2 (Table 7), and the same number of grid points for high intensities over $10 \text{ mm}\cdot\text{hr}^{-1}$.

A similar spatial distribution of precipitation accumulation between CTL and IRR is seen in the coastal area and in the centre of the Region 1, but negative differences (IRR minus CTL) appear in the north of Region 1 and in Region 2, mostly north of Region 2, indicating a decrease in rainfall amounts in the IRR case (Figure 8b,c). In addition, near the Ebro Delta (south of Region 1), precipitation accumulations are moved in space between simulation CTL and IRR (Figure 8b), as seen in alternating positive and negative grid points, as well as over the Mediterranean

TABLE 7 Convection-parametrized simulation results of precipitation accumulations (millimetres) per number of grid points n and number of grid points n exceeding rain rate (RR) of 3, 5, and 10 mm·hr $^{-1}$, considering all grid points or only irrigated (irr) grid points for Region 1 and Region 2 for Weather Research and Forecasting control (CTL) and irrigated (IRR) simulations for the 17-day period.

Region 1		Region 2				
Simulation	Amount (mm/n)	<i>n</i> for RR		Amount (mm/n)	<i>n</i> for RR	
		>3 mm·hr $^{-1}$	>5 mm·hr $^{-1}$		>3 mm·hr $^{-1}$	>5 mm·hr $^{-1}$
CTL all	17.16	3278	978	6	14.91	1101
IRR all	16.63	3108	922	6	12.62	997
CTL irr	16.04	2132	462	0	14.91	126
IRR irr	15.30	1986	426	0	12.62	105

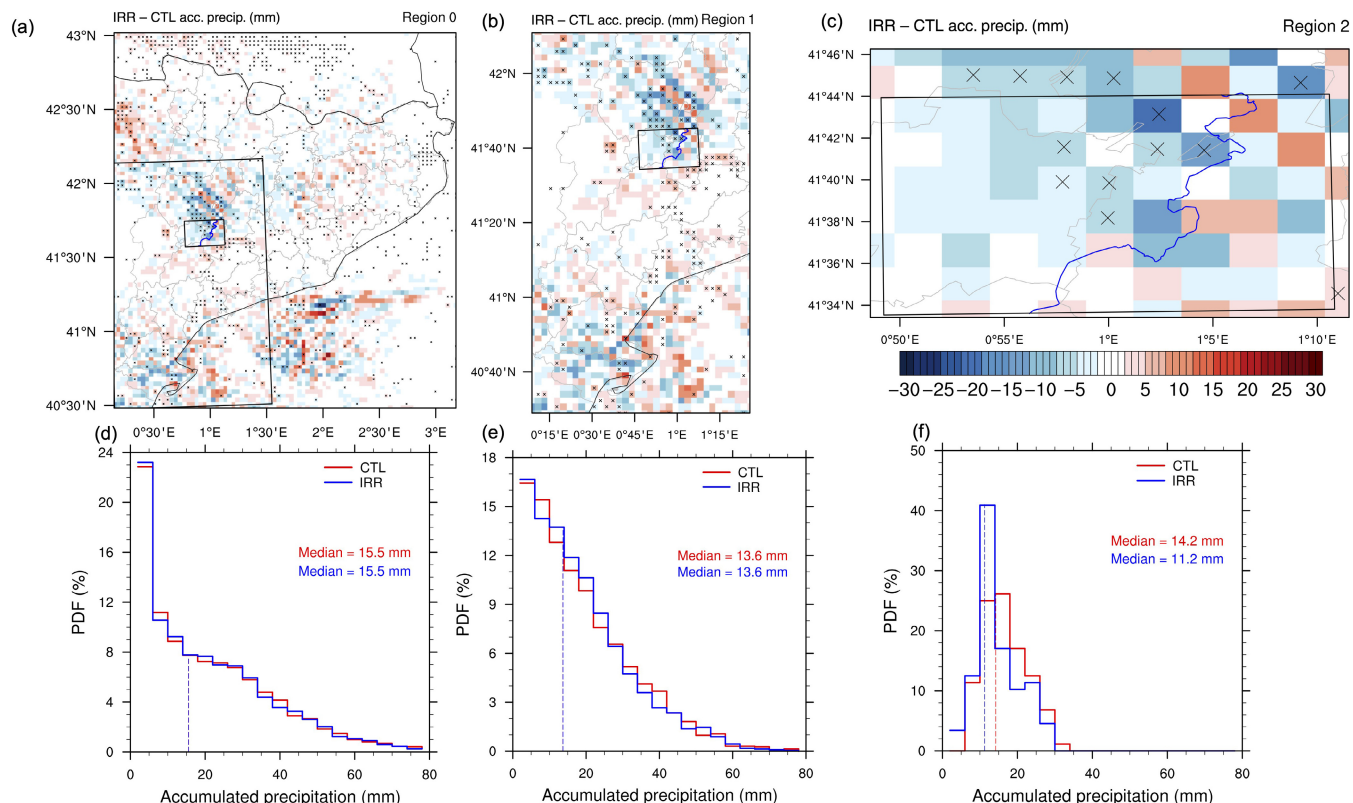


FIGURE 8 (a)–(c) Model results of accumulated precipitation differences (IRR minus CTL) in (a) Region 0, (b) Region 1, and (c) Region 2. (d)–(f) Modelled accumulated precipitation distributions in (d) Region 0, (e) Region 1, and (f) and Region 2 for CTL (red) and IRR (blue) simulations. Crosses in (c) indicate that the difference between CTL and IRR is statistically significant at the 95% confidence level using the Wilcoxon signed-rank test. CTL: Weather Research and Forecasting control simulation; IRR: Weather Research and Forecasting irrigated simulation; PDF: probability density function.

Sea (Figure 8a). Interestingly, spatial differences appear over non-irrigated areas, often located downwind from the irrigated ones, indicating a spatial displacement of the precipitation, but without a relevant increase or decrease of the total precipitation amount (Figure 8d,e). Although in Region 2 the rainfall amount is small according to the model, the distribution reveals larger accumulated precipitation amounts in the CTL run (Figure 8c,f), where the median of accumulated precipitation in the whole period decreases from 14.2 mm in CTL to 11.2 mm in IRR (see dashed line in Figure 8f). In Regions 0 and 1 there is

a low percentage of grid points, 7% and 9% respectively, where differences in precipitation are statistically significant, whereas in Region 2 the hourly accumulated precipitation differences are statistically significant (at the 95% confidence level) in 19% of the grid points (see crosses in Figure 8c). These grid points were mainly located west of the Urgell Channel, where the percentage of irrigation is higher. In addition, the number of grid points with precipitation greater than 3 or 5 mm·hr $^{-1}$ decreases by activating irrigation parametrization in Regions 1 and 2, either considering all grid points or only considering irrigated

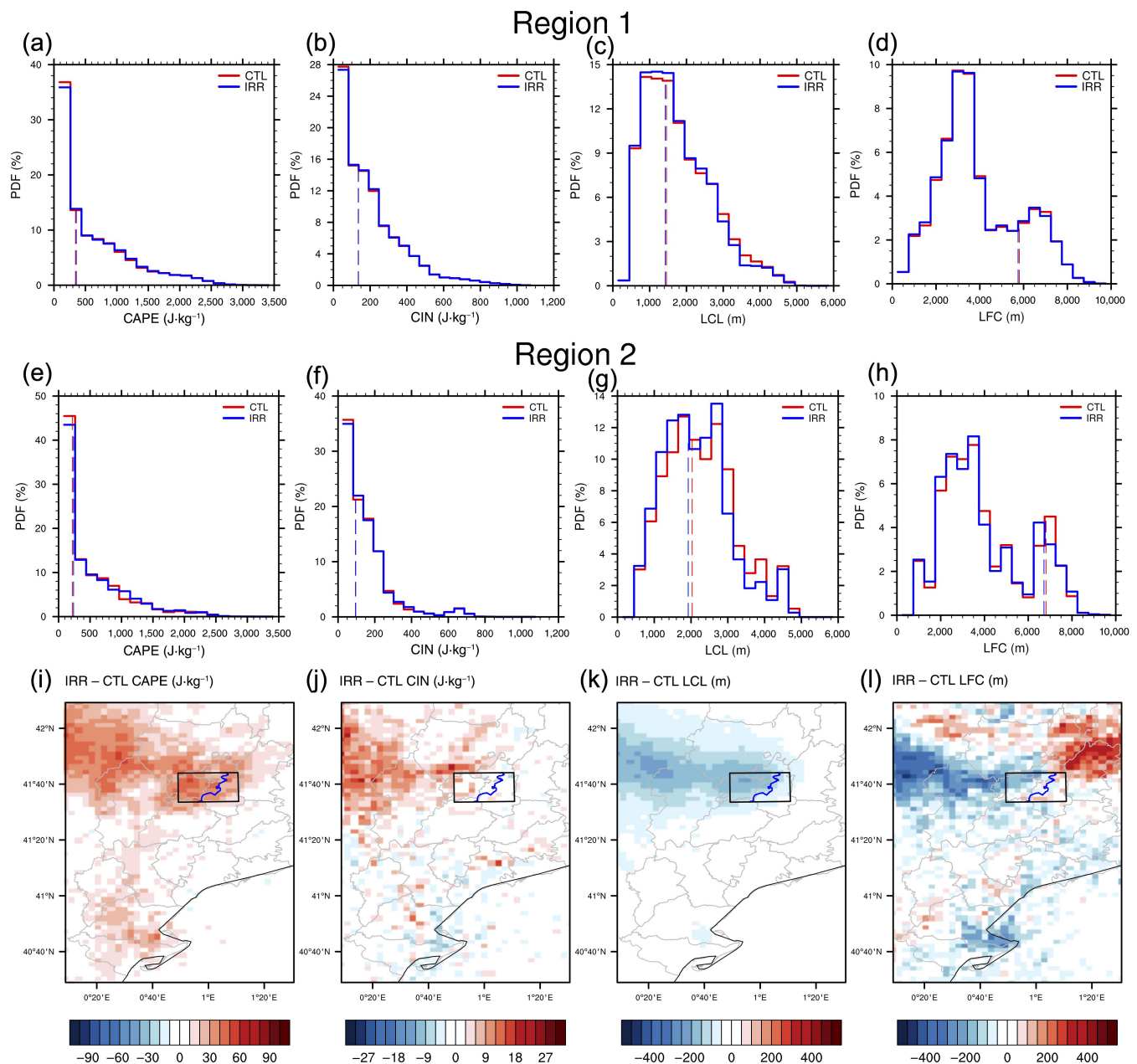


FIGURE 9 (a)–(h) Model results of convective available potential energy (CAPE), convective inhibition (CIN), lifting condensation level (LCL), and level of free convection (LFC) probability distributions for Weather Research and Forecasting control (CTL) and irrigated (IRR) simulations for grid points in (a–d) Region 1 and (e–h) Region 2. Red and blue dashed lines indicate the median values of the CTL and IRR simulations respectively. (i)–(l) Model spatial differences (IRR minus CTL) for the averaged CAPE, CIN, LCL, and LFC values. PDF: probability density function.

grid points (Table 7), revealing a reduction of the areas with moderate precipitation intensities when the land is irrigated.

Despite distributions of both the convective available potential energy (CAPE) and the convective inhibition (CIN) being relatively similar in CTL and IRR simulations (Figure 9a,b,e,f) they increase in IRR, mostly in the western area of Region 1, as the latent heat is greater due to irrigation. This is in accordance with the reduction in the

level of free convection (LFC; Figure 9d,h,l) and the lifting condensation level (LCL) in IRR (Figure 9c,g,k), which allows a greater integrated water vapour flux. In this case, the lower boundary-layer heights and higher CAPE values in IRR do not lead to rainfall increases locally, as discussed in Douglas *et al.*, 2009 and, on the contrary, precipitation accumulation is reduced when the surface is irrigated according to simulations. Spatially, when applying irrigation in the model it can be observed that the largest

increases in CAPE and CIN (Figure 9*i,j*) and decreases in LCL and LFC occur over the irrigated area (Figure 9*k,l*), near Region 2 and northwest of it. In contrast, increases in LFC appear northeast of Region 1.

4.3 | Sensitivity tests: Convection-permitting simulations

In order to explore the effects of convection parametrization in precipitation feedbacks, we run CTL and IRR convection-permitting simulations. Results from these simulations show nearly the same variations in near-surface air variables such as temperature, humidity, and wind speed as the previous ones (those including the convection parametrization). In contrast, the accumulated precipitation field simulated in convection-permitting runs is much lower than in the convection-parametrized ones, suggesting that at 3 km grid spacing the full vertical movements are not well resolved. The comparison of these simulations against observations shows that simulated precipitation is far from observed values for intensities over $1 \text{ mm}\cdot\text{day}^{-1}$ and that the impact of including irrigation in precipitation forecasts is negligible during the period studied (see Appendix B, Figure B.1). In fact, the effect upon precipitation of convective-permitting runs compared with convective-parametrized runs is much more relevant than the inclusion of irrigation parametrization. However, feedbacks between CTL and IRR simulations can still be explored. By activating the irrigation, the results show a change of sign in precipitation accumulation feedback in all regions when convection is not parametrized. That is, precipitation accumulations are larger in IRR than in CTL simulations in Region 2 (Table 8), the opposite from the previous results (Section 4.2). The precipitation accumulation in IRR increases in Region 0 and Region 2, by 1.3% and 7.8% respectively, whereas in Region 1 it decreases by 4.8%. Regarding precipitation intensities,

in convection-permitting simulations there is a decrease in the number of grid points where hourly precipitation intensity exceeds 3, 5, or $10 \text{ mm}\cdot\text{hr}^{-1}$ when activating irrigation. This would confirm the effect of irrigation in the lower atmosphere to inhibit convective processes, resulting in weaker precipitation intensities.

5 | DISCUSSION AND CONCLUSIONS

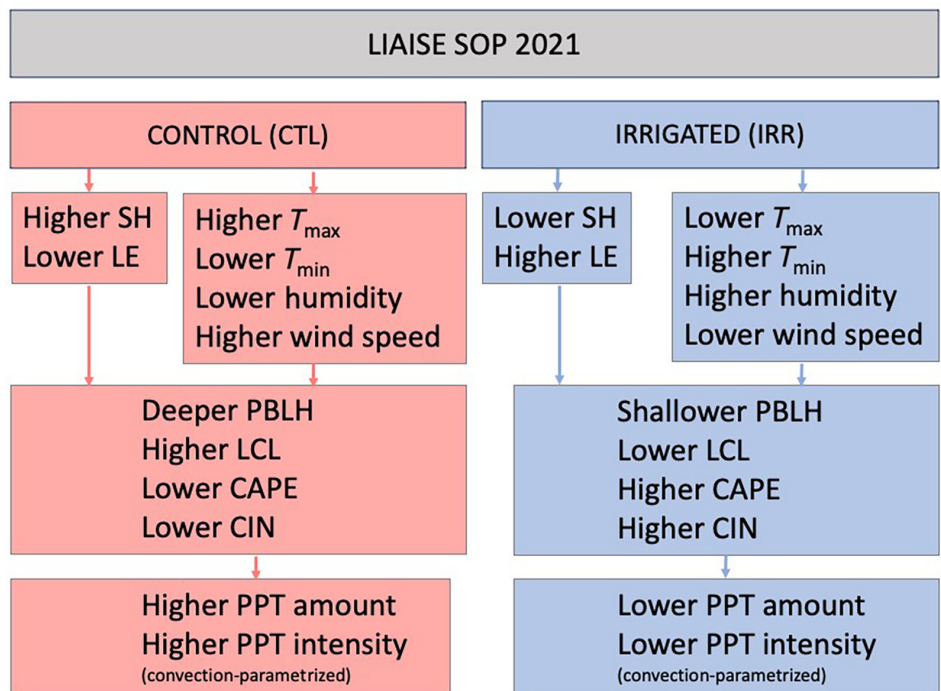
The results obtained here confirm the importance of including irrigation effects in WRF simulations in order to produce more precise and realistic forecasts of the main surface variables. Adding water to the soil in the model leads to an improved model forecast with a decrease in averaged near-surface air temperature, increase in humidity, decrease in wind speed, and shift in wind direction in the areas nearby where irrigation is applied. A general deceleration of the surface flow is produced when including the irrigation, especially in the sea breeze front. The surface energy balance is reversed, being dominated by the LE, and the boundary-layer height is then lowered in the area nearby where the irrigation is applied. Simulations including irrigation produce a decrease in the LCL and LFC, which also cause increases in CAPE and CIN (Figure 10).

We also conclude that the impact of irrigation upon precipitation depends on the activation of the convection parametrization or the use of convection-permitting runs. Simulations including cumulus parametrization are closer to observed rainfall amounts, and their response by including irrigation is a decrease (negative feedback) in precipitation accumulations for all regions and a reduction of the number of grid points with moderate hourly precipitation intensities. Given the increase in CAPE, these negative feedbacks in local precipitation could be revealing a disconnection between the local thermodynamic processes and the modelled precipitation. We speculate that such

TABLE 8 Convection-permitting (cp) simulation results of precipitation accumulations (millimetres) per number of grid points n and number of grid points n exceeding rain rate (RR) of 3, 5, and $10 \text{ mm}\cdot\text{hr}^{-1}$, considering all grid points or only irrigated (irr) grid points for Region 1 and Region 2 for Weather Research and Forecasting control (CTL) and irrigated (IRR) simulations for the 17-day period.

Region 1		Region 2			Region 2			
Simulation	Amount (mm/ n)	n for RR			Amount (mm/ n)	n for RR		
		$>3 \text{ mm}\cdot\text{hr}^{-1}$	$>5 \text{ mm}\cdot\text{hr}^{-1}$	$>10 \text{ mm}\cdot\text{hr}^{-1}$		$>3 \text{ mm}\cdot\text{hr}^{-1}$	$>5 \text{ mm}\cdot\text{hr}^{-1}$	$>10 \text{ mm}\cdot\text{hr}^{-1}$
CTL _{cp} all	5.05	11924	315	106	1.28	318	0	0
IRR _{cp} all	4.81	11857	272	79	1.38	337	0	0
CTL _{cp} irr	5.73	544	256	86	1.28	0	0	0
IRR _{cp} irr	5.49	543	223	63	1.38	0	0	0

FIGURE 10 A simplified conceptual model of the impact of irrigation in Weather Research and Forecasting simulations during LIAISE special observation period (SOP; July 15–31, 2021) considering control (CTL) and irrigated (IRR) runs. Selected atmospheric variables include surface sensible heat flux (SH), surface latent heat flux (LE), daily maximum surface air temperature (T_{\max}), daily minimum surface air temperature (T_{\min}), air surface specific humidity (q), air surface wind speed, planetary boundary-layer height (PBLH), lifting condensation level (LCL), convective available potential energy (CAPE), convection inhibition (CIN), and precipitation (PPT).



disconnection could be influenced by the fact that during the LIAISE SOP the precipitation systems were forced by larger scale systems rather than formed or modified nearby the irrigated areas.

The representation of surface fluxes is improved when including irrigation as well, with a larger fraction of energy invested in LE rather than in SH. This helps resolving more realistically the land-atmosphere heat transfer during the day, but it is still poorly resolved at night as the soil temperature is too underestimated and the minimum air surface temperatures are overestimated as well. The results in that sense point out the need of a revision of representation of cooling processes in wet soil conditions in land-surface models, including the possible reduction of the surface albedo caused by irrigation (Yang *et al.*, 2020a), whose effect is not included in this study. On the other hand, the inability of the model to reproduce the extreme LE values points out the need to define the scale and representativity of flux measurements across the different spatial scales in the extreme heterogeneous area of LIAISE (Mangan *et al.*, 2023a) and how this should be compared with the model resolved scales.

The results obtained are in accordance with similar previous model-based experiments in the United States (Pei *et al.*, 2016; Whitesel *et al.*, 2024; Yang *et al.*, 2017). The final decrease in rainfall over the irrigated region was also the outcome of a case study in the Great Plains (Whitesel *et al.*, 2024), although different land uses also impacted the development of the subsequent precipitation. The observed weakening in the sea breeze flow entrance near the LIAISE region is also a common feature found in previous studies, revealing modifications in terrain-forced

circulations (Phillips *et al.*, 2022) or the modification of the Great Plains low-level jet intensity (Huber *et al.*, 2014; Pei *et al.*, 2016; Yang *et al.*, 2020b). Similarly, shallower PBLH and lower LCL and LFC were obtained over the irrigated areas in Great Plains Irrigation Experiment campaign (Lachenmeier *et al.*, 2023).

In accordance with Zittis *et al.* (2018), the application of nudging was necessary to simulate rainfall during the period. Despite this, the precipitation field reproduced with explicit-convection simulations (without cumulus parametrization) revealed a poor comparison against observations and radar QPEs, as it was highly underestimated and most of the precipitation events were not captured, in both large Region 0 and small Region 2. Additional simulation tests using scale-aware convective parametrization also revealed too underestimated precipitation accumulations. Therefore, in our 3 km grid spacing simulations (falling at the grey-zone resolution), it was necessary to activate the convection scheme to reproduce precipitation systems closer to reality. However, as found by Taylor *et al.* (2013), soil moisture feedbacks on precipitation can vary in simulations if convection parametrization is activated or not. In our case, a negative feedback of irrigation on precipitation is obtained in simulations where convection is activated, whereas convection-permitting simulations lead to a positive feedback in terms of precipitation accumulation near the irrigated area, as found similarly by Valmassoi *et al.* (2020b).

According to the model results, we conclude that the thermodynamic properties of the lower atmosphere are highly modified and improved when the soil is irrigated, whereas feedbacks in rainfall are not so clear. In addition,

including the irrigation parametrization did not improve the representation of the observed precipitation field, as revealed in the verification against observations from weather radar and rain-gauges. A possible explanation is that the influence of land-atmosphere processes upon precipitation systems during the LIAISE SOP studied here were relatively limited, as the precipitation systems mostly did not form directly over the irrigated area of Region 2 during the period studied. Instead, the precipitation systems observed formed elsewhere and seem to be driven by large-scale or mesoscale circulations. As the model was generally not able to reproduce the precipitation convective systems observed in terms of location and timing, another limitation may come from the difficulties to resolve the interaction between different scales, from local to landscape and regional (Mangan *et al.*, 2023b). In that sense, future research should focus on selected precipitation case studies modified by local conditions or triggered by lower atmospheric processes and the proper model resolving interactions across scales. In addition, a better representation of the Ebro basin irrigated areas in the model, including more realistic irrigation data (different hours of irrigation, specific water amounts in each field type, etc.), should also be considered to evaluate possible further improvement of operational forecasts.

ACKNOWLEDGEMENTS

We thank the hosts, organizers, and participants of the LIAISE campaign. We specially thank Aaron Boone for his advice and suggestions and Guylaine Canut for providing the data from La Cendrosa. This work was partly funded by the projects MCIN/AEI/10.13039/501100011033 (PID2021-124253OB-I00(ARTEMIS) : RTI2018-098693-B-C32(WISE-PreP)), and the Water Research Institute (IdRA) of the University of Barcelona.

CONFLICT OF INTEREST STATEMENT

The authors have no conflicts of interest to declare.

DATA AVAILABILITY STATEMENT

Data collected during the LIAISE campaign are archived at <https://liaise.aeris-data.fr/>. Owing to the nature of the experiment, data are not yet available for public download. Data can be provided directly from the authors upon request.

ORCID

- Mireia Udina  <https://orcid.org/0000-0002-8024-3293>
- Eric Peinó  <https://orcid.org/0000-0003-4381-4875>
- Francesc Polls  <https://orcid.org/0000-0001-8900-4590>
- Jordi Mercader  <https://orcid.org/0000-0003-4886-9656>
- Arianna Valmassoi  <https://orcid.org/0000-0003-2215-3983>

Alexandre Paci  <https://orcid.org/0000-0002-7917-8711>
 Joan Bech  <https://orcid.org/0000-0003-3597-7439>

REFERENCES

- Asmus, C., Hoffmann, P., Pietikäinen, J.-P., Böhner, J. & Rechid, D. (2023) Modeling and evaluating the effects of irrigation on land-atmosphere interaction in South-West Europe with the regional climate model REMO2020-iMOVE using a newly developed parameterization. *EGU Sphere*, 2023, 1–39 <https://egusphere.copernicus.org/preprints/2023/egusphere-2023-890/>
- Barton, E.J., Taylor, C., Mitra, A. & Jayakumar, A. (2023) Systematic daytime increases in atmospheric biases linked to dry soils in irrigated areas in Indian operational forecasts. *Atmospheric Science Letters*, 24(9), e1172.
- Barton, E.J., Taylor, C.M., Parker, D.J., Turner, A.G., Belušić, D. & Böing, S.J. (2020) A case-study of land-atmosphere coupling during monsoon onset in northern India. *Quarterly Journal of the Royal Meteorological Society*, 146, 2891–2905.
- Bech, J., Arús, J., Castán, S., Pineda, N., Rigo, T. & Montanyà, J. (2015) A study of the 21 March 2012 tornadic quasi linear convective system in Catalonia. *Atmospheric Research*, 158, 192–209.
- Bech, J., Rigo, T., Pineda, N., Segalà, S., Vilaclara, E., Sánchez-Diezma, R. et al. (2005) Implementation of the EHIMI software package in the weather radar operational chain of the catalan meteorological service. Proceedings 32 nd international conference on radar meteorology, Albuquerque, NM, USA.
- Boone, A., Bellvert, J., Best, M., Brooke, J., Canut-Rocafoft, G., Cuxart, J. et al. (2021) Updates on the international land surface interactions with the atmosphere over the iberian semi-arid environment (LIAISE) field campaign. <https://hal.science/hal-03842003/document>
- Brooke, J.K., Best, M.J., Lock, A.P., Osborne, S.R., Price, J., Cuxart, J. et al. (2023) Irrigation contrasts through the morning transition. *Quarterly Journal of the Royal Meteorological Society*, 150(758), 170–194. <https://rmets.onlinelibrary.wiley.com/doi/abs/10.1002/qj.4590>
- Canut, G. (2022) LIAISE LA-CENDROSA CNRM MTO-FLUX-30MIN L2. Aeris <https://doi.org/10.25326/320>
- Copernicus Climate Change Service (C3S). (2017) ERA5: Fifth generation of ECMWF atmospheric reanalyses of the global climate. <https://climate.copernicus.eu/climate-reanalysis>
- Cuxart, J. & Boone, A. (2020) Evapotranspiration over land from a boundary-layer meteorology perspective. *Boundary-Layer Meteorology*, 177, 427–459.
- Dari, J., Brocca, L., Modanesi, S., Massari, C., Tarpanelli, A. & Barbetta, S. (2023) Regional data sets of high-resolution (1 and 6 km) irrigation estimates from space. *Earth System Science Data*, 15, 1555–1575.
- de Vrese, P. & Hagemann, S. (2018) Uncertainties in modelling the climate impact of irrigation. *Climate Dynamics*, 51, 2023–2038.
- DeAngelis, A., Dominguez, F., Fan, Y., Robock, A., Kustu, M.D. & Robinson, D. (2010) Evidence of enhanced precipitation due to irrigation over the Great Plains of the United States. *Journal of Geophysical Research: Atmospheres*, 115, D15115.
- Douglas, E., Beltrán-Przekurat, A., Niyogi, D., Pielke, R., Sr. & Vörösmarty, C. (2009) The impact of agricultural intensification and irrigation on land-atmosphere interactions and indian monsoon precipitation—a mesoscale modeling perspective. *Global and Planetary Change*, 67, 117–128.

- Douglas, E.M., Niyogi, D., Frolking, S., Yeluripati, J.B., Pielke, R.A., Sr. & Niyogi, N. (2006) Changes in moisture and energy fluxes due to agricultural land use and irrigation in the Indian Monsoon Belt. *Geophysical Research Letters*, 33, L14403.
- Dudhia, J. (1989) Numerical study of convection observed during the winter monsoon experiment using a mesoscale two-dimensional model. *Journal of Atmospheric Sciences*, 46, 3077–3107.
- Ebert, E.E. (2008) Fuzzy verification of high-resolution gridded forecasts: a review and proposed framework. *Meteorological Applications: A Journal of Forecasting, Practical Applications, Training Techniques and Modelling*, 15, 51–64.
- Eyring, V., Bony, S., Meehl, G.A., Senior, C.A., Stevens, B. & Stouffer, R.J. (2016) Overview of the coupled model Intercomparison project phase 6 (CMIP6) experimental design and organization. *Geoscientific Model Development*, 9, 1937–1958.
- Fan, Y., Im, E.-S., Lan, C.-W. & Lo, M.-H. (2023) An increase in precipitation driven by irrigation over the North China plain based on RegCM and WRF simulations. *Journal of Hydrometeorology*, 24, 1155–1173.
- Farnell, C., Rigo, T. & Heymsfield, A. (2022) Shape of hail and its thermodynamic characteristics related to records in Catalonia. *Atmospheric Research*, 271, 106098.
- Fletcher, J., Birch, C., Keane, R., Taylor, C. & Folwell, S. (2022) The effect of ganges river basin irrigation on pre-monsoon rainfall. *Quarterly Journal of the Royal Meteorological Society*, 148, 3056–3070.
- Gonzalez, S., Callado, A., Werner, E., Escribà, P. & Bech, J. (2018) Coastally trapped disturbances caused by the tramontane wind on the northwestern Mediterranean: numerical study and sensitivity to short-wave radiation. *Quarterly Journal of the Royal Meteorological Society*, 144, 1321–1336.
- Guillod, B.P., Orlowsky, B., Miralles, D.G., Teuling, A.J. & Seneviratne, S.I. (2015) Reconciling spatial and temporal soil moisture effects on afternoon rainfall. *Nature Communications*, 6, 1–6.
- Hersbach, H., Bell, B., Berrisford, P., Hirahara, S., Horányi, A. & Muñoz-Sabater, J. (2020) The ERA5 global reanalysis. *Quarterly Journal of the Royal Meteorological Society*, 146, 1999–2049.
- Hong, S.-Y., Dudhia, J. & Chen, S.-H. (2004) A revised approach to ice microphysical processes for the bulk parameterization of clouds and precipitation. *Monthly Weather Review*, 132, 103–120.
- Hong, S.-Y., Noh, Y. & Dudhia, J. (2006) A new vertical diffusion package with an explicit treatment of entrainment processes. *Monthly Weather Review*, 134, 2318–2341.
- Horvath, K., Šepić, J. & Prtenjak, M.T. (2018) Atmospheric forcing conducive for the Adriatic 25 june 2014 meteotsunami event. *Pure and Applied Geophysics*, 175, 3817–3837.
- Huber, D.B., Mechem, D.B. & Brunsell, N.A. (2014) The effects of Great Plains irrigation on the surface energy balance, regional circulation, and precipitation. *Climate*, 2, 103–128.
- Irwin, J.S. (1979) A theoretical variation of the wind profile power-law exponent as a function of surface roughness and stability. *Atmospheric Environment*, 13, 191–194.
- Jeworrek, J., West, G. & Stull, R. (2019) Evaluation of cumulus and microphysics parameterizations in WRF across the convective gray zone. *Weather and Forecasting*, 34, 1097–1115.
- Jeworrek, J., West, G. & Stull, R. (2021) WRF precipitation performance and predictability for systematically varied parameterizations over complex terrain. *Weather and Forecasting*, 36, 893–913.
- Jiménez, M.A., Grau, A., Martínez-Villagrassa, D. & Cuxart, J. (2023) Characterization of the marine-air intrusion Marinada in the eastern Ebro sub-basin. *International Journal of Climatology*, 43, 7682–7699. <https://rmets.onlinelibrary.wiley.com/doi/abs/10.1002/joc.8287>
- Jiménez, P.A., Dudhia, J., González-Rouco, J.F., Navarro, J., Montávez, J.P. & García-Bustamante, E. (2012) A revised scheme for the WRF surface layer formulation. *Monthly Weather Review*, 140, 898–918.
- Jolliffe, I.T. & Stephenson, D.B. (2012) *Forecast verification: a practitioner's guide in atmospheric science*. Oxford: John Wiley & Sons.
- Kain, J.S. (2004) The Kain-Fritsch convective parameterization: an update. *Journal of Applied Meteorology*, 43, 170–181.
- Kueppers, L.M., Snyder, M.A. & Sloan, L.C. (2007) Irrigation cooling effect: regional climate forcing by land-use change. *Geophysical Research Letters*, 34, L03703.
- Lachenmeier, E., Mahmood, R., Phillips, C., Nair, U., Rappin, E. & Pielke, R.A., Sr. (2023) Irrigated agriculture significantly modifies seasonal boundary layer atmosphere and lower tropospheric convective environment. *Journal of Applied Meteorology and Climatology*, 63, 245–262.
- Lavers, D.A., Simmons, A., Vamborg, F. & Rodwell, M.J. (2022) An evaluation of ERA5 precipitation for climate monitoring. *Quarterly Journal of the Royal Meteorological Society*, 148, 3152–3165.
- Lawston, P.M., Santanello, J.A., Hanson, B. & Arsensault, K. (2020) Impacts of irrigation on summertime temperatures in the Pacific northwest. *Earth Interactions*, 24, 1–26.
- Lawston-Parker, P., Santanello, J.A., Jr. & Chaney, N.W. (2023) Investigating the response of land-atmosphere interactions and feedbacks to spatial representation of irrigation in a coupled Modeling framework. *EGUphere*, 2023, 1–31.
- Lee, E., Chase, T.N., Rajagopalan, B., Barry, R.G., Biggs, T.W. & Lawrence, P.J. (2009) Effects of irrigation and vegetation activity on early Indian summer monsoon variability. *International Journal of Climatology: A Journal of the Royal Meteorological Society*, 29, 573–581.
- Lee, K.-O., Flamant, C., Ducrocq, V., Duffourg, F., Fourrié, N. & Delanoë, J. (2017) Initiation and development of a mesoscale convective system in the Ebro River valley and related heavy precipitation over northeastern Spain during HyMeX IOP 15a. *Quarterly Journal of the Royal Meteorological Society*, 143, 942–956.
- Li, W., He, X., Sun, W., Scaioni, M., Yao, D. & Fu, J. (2019) Evaluating three satellite-based precipitation products of different spatial resolutions in Shanghai based on upscaling of rain gauge. *International Journal of Remote Sensing*, 40, 5875–5891.
- Mahmood, R., Pielke, R.A., Sr., Hubbard, K.G., Niyogi, D., Dirmeyer, P.A. & McAlpine, C. (2014) Land cover changes and their biogeophysical effects on climate. *International Journal of Climatology*, 34, 929–953.
- Mangan, M.R., Hartogensis, O., Boone, A., Branch, O., Canut, G. & Cuxart, J. (2023a) The surface-boundary layer connection across spatial scales of irrigation-driven thermal heterogeneity: an integrated data and modeling study of the LIAISE field campaign. *Agricultural and Forest Meteorology*, 335, 109452.
- Mangan, M.R., Hartogensis, O., van Heerwaarden, C. & Vilà-Guerau de Arellano, J. (2023b) Evapotranspiration controls across spatial scales of heterogeneity. *Quarterly Journal of the Royal Meteorological Society*, 149(756), 2696–2718.
- Mastrangelo, D., Horvath, K., Riccio, A. & Miglietta, M. (2011) Mechanisms for convection development in a long-lasting heavy precipitation event over southeastern Italy. *Atmospheric Research*, 100, 586–602.

- Maurer, V., Kalthoff, N. & Gantner, L. (2015) Predictability of convective precipitation for West Africa: does the land surface influence ensemble variability as much as the atmosphere? *Atmospheric Research*, 157, 91–107.
- McDermid, S., Nocco, M. & Lawston-Parker, P. (2023) Irrigation in the earth system. *Nature Reviews Earth and Environment*, 4, 435–453.
- Mercader, J., Codina, B., Sairouni, A. & Cunillera, J. (2010) Results of the meteorological model WRF-ARW over Catalonia, using different parameterizations of convection and cloud microphysics. *Tethys: Journal of Mediterranean Meteorology & Climatology*, 2010(7), 75–86.
- Mlawer, E.J., Taubman, S.J., Brown, P.D., Iacono, M.J. & Clough, S.A. (1997) Radiative transfer for inhomogeneous atmospheres: RRTM, a validated correlated-k model for the longwave. *Journal of Geophysical Research*, 102, 16616–16663.
- Moiwo, J.P. & Tao, F. (2015) Contributions of precipitation, irrigation and soil water to evapotranspiration in (semi)-arid regions. *International Journal of Climatology*, 35, 1079–1089.
- Pei, L., Moore, N., Zhong, S., Kendall, A.D., Gao, Z. & Hyndman, D.W. (2016) Effects of irrigation on summer precipitation over the United States. *Journal of Climate*, 29, 3541–3558. <https://journals.ametsoc.org/view/journals/clim/29/10/jcli-d-15-0337.1.xml>
- Phillips, C., Nair, U., Mahmood, R., Rappin, E. & Pielke, R., Sr. (2022) Influence of irrigation on diurnal mesoscale circulations: results from GRAINEX. *Geophysical Research Letters*, 49, e2021GL096822.
- Pielke, R.A., Mahmood, R. & McAlpine, C. (2016) Land's complex role in climate change. *Physics Today*, 69, 40.
- Pielke, R.A., Pitman, A., Niyogi, D., Mahmood, R., McAlpine, C. & Hossain, F. (2011) Land use/land cover changes and climate: modeling analysis and observational evidence. *Wiley Interdisciplinary Reviews: Climate Change*, 2, 828–850.
- Prein, A.F., Langhans, W., Fosser, G., Ferrone, A., Ban, N. & Goergen, K. (2015) A review on regional convection-permitting climate modeling: demonstrations, prospects, and challenges. *Reviews of Geophysics*, 53, 323–361.
- Qian, Y., Yang, Z., Feng, Z., Liu, Y., Gustafson, W.I. & Berg, L.K. (2020) Neglecting irrigation contributes to the simulated summertime warm-and-dry bias in the central United States. *Npj Climate and Atmospheric Science*, 3, 31.
- Rappin, E., Mahmood, R., Nair, U., Pielke, R.A., Sr., Brown, W. & Oncley, S. (2021) The Great Plains irrigation experiment (GRAINEX). *Bulletin of the American Meteorological Society*, 102, E1756–E1785.
- Rigo, T., Llasat, M.C. & Esbrí, L. (2021) The results of applying different methodologies to 10 years of quantitative precipitation estimation in Catalonia using weather radar. *Geomatics*, 1, 347–368.
- Sacks, W.J., Cook, B.I., Buenning, N., Levis, S. & Helkowski, J.H. (2009) Effects of global irrigation on the near-surface climate. *Climate Dynamics*, 33, 159–175.
- Saeed, F., Hagemann, S. & Jacob, D. (2009) Impact of irrigation on the south Asian summer monsoon. *Geophysical Research Letters*, 36, L20711.
- Semeena, V.S., Klein, C., Taylor, C.M. & Webster, S. (2023) Impact of land surface processes on convection over West Africa in convection-permitting ensemble forecasts: a case study using the MOGREPS ensemble. *Atmospheric Science Letters*, 24(8), e1167.
- Siebert, S., Henrich, V., Frenken, K. & Burke, J. (2013) Global map of irrigation areas version 5. Rheinische Friedrich-Wilhelms-university. Bonn, Germany/Food and Agriculture Organization of the United Nations, Rome, Italy, 2, 1299–1327.
- Skamarock, W.C., Klemp, J.B., Dudhia, J., Gill, D.O., Liu, Z. & Berner, J. (2021) *A description of the advanced research WRF model version 4.3 (No. NCAR/TN-556+STR)*. Boulder, CO: National Center for Atmospheric Research (NCAR).
- Steeneveld, G.-J. & Peerlings, E.E. (2020) Mesoscale model simulation of a severe summer thunderstorm in the Netherlands: performance and uncertainty assessment for parameterised and resolved convection. *Atmosphere*, 11, 811.
- Taylor, C.M., Birch, C.E., Parker, D.J., Dixon, N., Guichard, F. & Nikulin, G. (2013) Modeling soil moisture-precipitation feedback in the sahel: importance of spatial scale versus convective parameterization. *Geophysical Research Letters*, 40, 6213–6218.
- Taylor, C.M., de Jeu, R.A., Guichard, F., Harris, P.P. & Dorigo, W.A. (2012) Afternoon rain more likely over drier soils. *Nature*, 489, 423–426.
- Tewari, M., Chen, F., Wang, W., Dudhia, J., LeMone, M., Mitchell, K. et al. (2004) Implementation and verification of the unified NOAH land surface model in the WRF model (formerly paper number 17.5). Proceedings of the 20th conference on weather analysis and forecasting/16th conference on numerical weather prediction, Seattle, WA, USA, vol. 14.
- Thiery, W., Davin, E.L., Lawrence, D.M., Hirsch, A.L., Hauser, M. & Seneviratne, S.I. (2017) Present-day irrigation mitigates heat extremes. *Journal of Geophysical Research: Atmospheres*, 122, 1403–1422.
- Trapero, L., Bech, J., Duffourg, F., Esteban, P. & Lorente, J. (2013) Mesoscale numerical analysis of the historical November 1982 heavy precipitation event over Andorra (eastern Pyrenees). *Natural Hazards and Earth System Sciences*, 13, 2969–2990.
- Trapero, L., Bech, J., Rigo, T., Pineda, N. & Forcadell, D. (2009) Uncertainty of precipitation estimates in convective events by the meteorological Service of Catalonia radar network. *Atmospheric Research*, 93, 408–418.
- Turner, A.G., Bhat, G., Martin, G., Parker, D.J., Taylor, C. & Mitra, A.K. (2020) Interaction of convective organization with monsoon precipitation, atmosphere, surface and sea: the 2016 INCOMPASS field campaign in India. *Quarterly Journal of the Royal Meteorological Society*, 146, 2828–2852.
- Tuttle, S. & Salvucci, G. (2016) Empirical evidence of contrasting soil moisture-precipitation feedbacks across the United States. *Science*, 352, 825–828.
- Udina, M., Soler, M.R. & Sol, O. (2017) A modeling study of a trapped lee-wave event over the Pyrénées. *Monthly Weather Review*, 145, 75–96.
- Valmassoi, A., Dudhia, J., Di Sabatino, S. & Pilla, F. (2020a) Evaluation of three new surface irrigation parameterizations in the WRF-ARW v3.8.1 model: the Po Valley (Italy) case study. *Geoscientific Model Development*, 13, 3179–3201.
- Valmassoi, A., Dudhia, J., Di Sabatino, S. & Pilla, F. (2020b) Irrigation impact on precipitation during a heatwave event using WRF-ARW: the summer 2015 Po Valley case. *Atmospheric Research*, 241, 104951.
- Valmassoi, A. & Keller, J.D. (2022) A review on irrigation parameterizations in earth system models. *Frontiers in Water*, 4, 906664.

- Van Baelen, J., Reverdy, M., Tridon, F., Labbouz, L., Dick, G., Bender, M. et al. (2011) On the relationship between water vapour field evolution and the life cycle of precipitation systems. *Quarterly Journal of the Royal Meteorological Society*, 137, 204–233.
- Van Osnabrugge, B., Weerts, A. & Uijlenhoet, R. (2017) genRE: a method to extend gridded precipitation climatology data sets in near real-time for hydrological forecasting purposes. *Water Resources Research*, 53, 9284–9303.
- Wang, W., Barker, D., Bray, J., Bruyere, C., Duda, M., Dudhia, J. et al. (2007) User's guide for advanced research WRF (ARW) modeling system version 3. Mesoscale and microscale meteorology division–National Center for Atmospheric Research (MMM-NCAR).
- Whitesel, D., Mahmood, R., Flanagan, P., Rappin, E., Nair, U. & Pielke, R.A., Sr. (2024) Impacts of irrigation on a precipitation event during GRAINEX in the High Plains aquifer region. *Agricultural and Forest Meteorology*, 345, 109854.
- Woolson, R.F. (2008) Wilcoxon Signed-Rank Test. In *Wiley Encyclopedia of Clinical Trials* (eds R.B. D'Agostino, L. Sullivan and J. Massaro). <https://doi.org/10.1002/9780471462422.eoct979>
- Yang, Q., Huang, X. & Tang, Q. (2020a) Global assessment of the impact of irrigation on land surface temperature. *Scientific Bulletin*, 65, 1440–1443.
- Yang, Y., Roderick, M.L., Guo, H., Miralles, D.G., Zhang, L. & Fatichi, S. (2023) Evapotranspiration on a greening earth. *Nature Reviews Earth & Environment*, 4, 626–641.
- Yang, Z., Dominguez, F., Zeng, X., Hu, H., Gupta, H. & Yang, B. (2017) Impact of irrigation over the California Central Valley on regional climate. *Journal of Hydrometeorology*, 18, 1341–1357 <https://journals.ametsoc.org/view/journals/hdr/18/5/jhm-d-16-0158.1.xml>
- Yang, Z., Qian, Y., Liu, Y., Berg, L.K., Gustafson, W.I. & Feng, Z. (2020b) Understanding irrigation impacts on low-level jets over the great plains. *Climate Dynamics*, 55, 925–943.
- Yang, Z., Qian, Y., Liu, Y., Berg, L.K., Hu, H., Dominguez, F. et al. (2019) Irrigation impact on water and energy cycle during dry years over the United States using convection-permitting WRF and a dynamical recycling model. *Journal of Geophysical Research: Atmospheres*, 124, 11220–11241. <https://agupubs.onlinelibrary.wiley.com/doi/abs/10.1029/2019JD030524>
- Zaveri, E. & Lobell, D.B. (2019) The role of irrigation in changing wheat yields and heat sensitivity in India. *Nature Communications*, 10, 4144.
- Zepeda-Arce, J., Foufoula-Georgiou, E. & Droege, K.K. (2000) Space-time rainfall organization and its role in validating quantitative precipitation forecasts. *Journal of Geophysical Research: Atmospheres*, 105, 10129–10146.
- Zittis, G., Bruggeman, A., Hadjinicolaou, P., Camera, C. & Lelieveld, J. (2018) Effects of meteorology nudging in regional hydroclimatic simulations of the eastern Mediterranean. *Atmosphere*, 9, 470.

How to cite this article: Udina, M., Peinó, E., Polls, F., Mercader, J., Guerrero, I., Valmassoi, A. et al. (2024) Irrigation impact on boundary layer and precipitation characteristics in Weather Research and Forecasting model simulations during LIAISE-2021. *Quarterly Journal of the Royal Meteorological Society*, 150(763), 3251–3273.
Available from: <https://doi.org/10.1002/qj.4756>

APPENDIX A. CONTINGENCY TABLE

A standard contingency (Table A.1) was used to compute the categorical statistics in Table 3, defining categorical events upon exceedance of a threshold of precipitation amount comparing simulations and observations (EHIMI).

TABLE A.1 Contingency table used to calculate the categorical statistics summarized in Table 3.

	EHIMI \geq threshold	EHIMI $<$ threshold
Simulation \geq threshold	Hits	False alarms
Simulation $<$ threshold	Misses	Correct negatives

Abbreviation: EHIMI, hydrometeorological integrated forecasting tool.

APPENDIX B. VERIFICATION OF PRECIPITATION IN CONVECTION-PERMITTING SIMULATIONS

The categorical statistics for convection-permitting simulations are shown in Figure B.1 for Region 0 and Region 2 and for the two simulations CTL and IRR, splitting the results among five different spatial scales and six different daily precipitation intensity thresholds. The HK scores for Region 0 are poorer than in convection-parametrized simulations for all precipitation intensity thresholds. For Region 2, low precipitation intensities from 0.1 to 1 mm·day⁻¹ are better resolved in convection-permitting simulations, although higher thresholds are not resolved, with almost all scores being close to zero. Differences between rainfall forecasts of CTL and IRR convection-permitting simulations are negligible in both regions, suggesting that precipitation processes are not improved by the surface changes induced by irrigation.

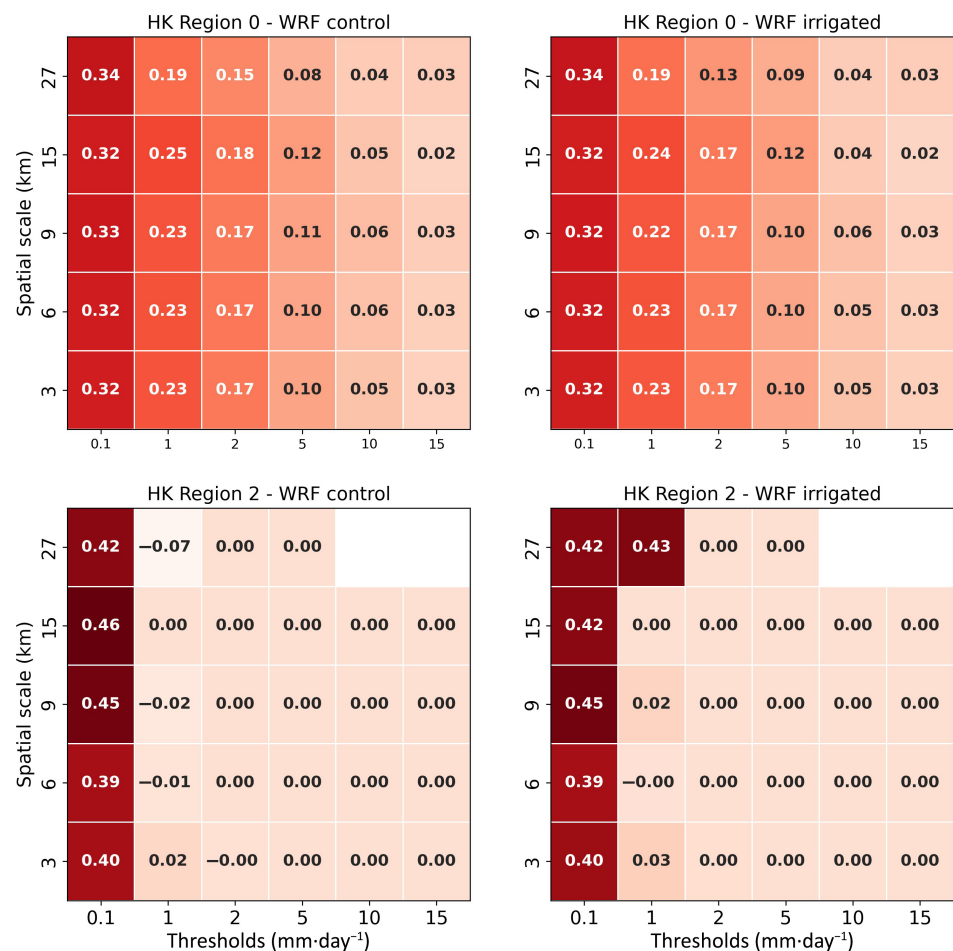


FIGURE B.1 Hansen and Kuipers (HK) scores for the Region 0 (top row) and Region 2 (bottom row) separating Weather Research and Forecasting (WRF) control (left column) and irrigated (right column) simulations against quantitative precipitation estimates, including different spatial resolution aggregations and different intensity thresholds, using convection-permitting simulations. The darker (lighter) colour indicates good (poor) performance according to the decision model used by the upscaling method.

APPENDIX C. DAILY PRECIPITATION IN CONVECTION-PARAMETRIZED SIMULATIONS

According to the EHIMI QPEs, there were four days with significant precipitation accumulation during July 2021 in

Region 0 (July 20, 26, 30, and 31), as shown in Figure C.1. The spatial distribution of the daily precipitation field can be compared with the simulation outputs CTL and IRR (Figure C.1).

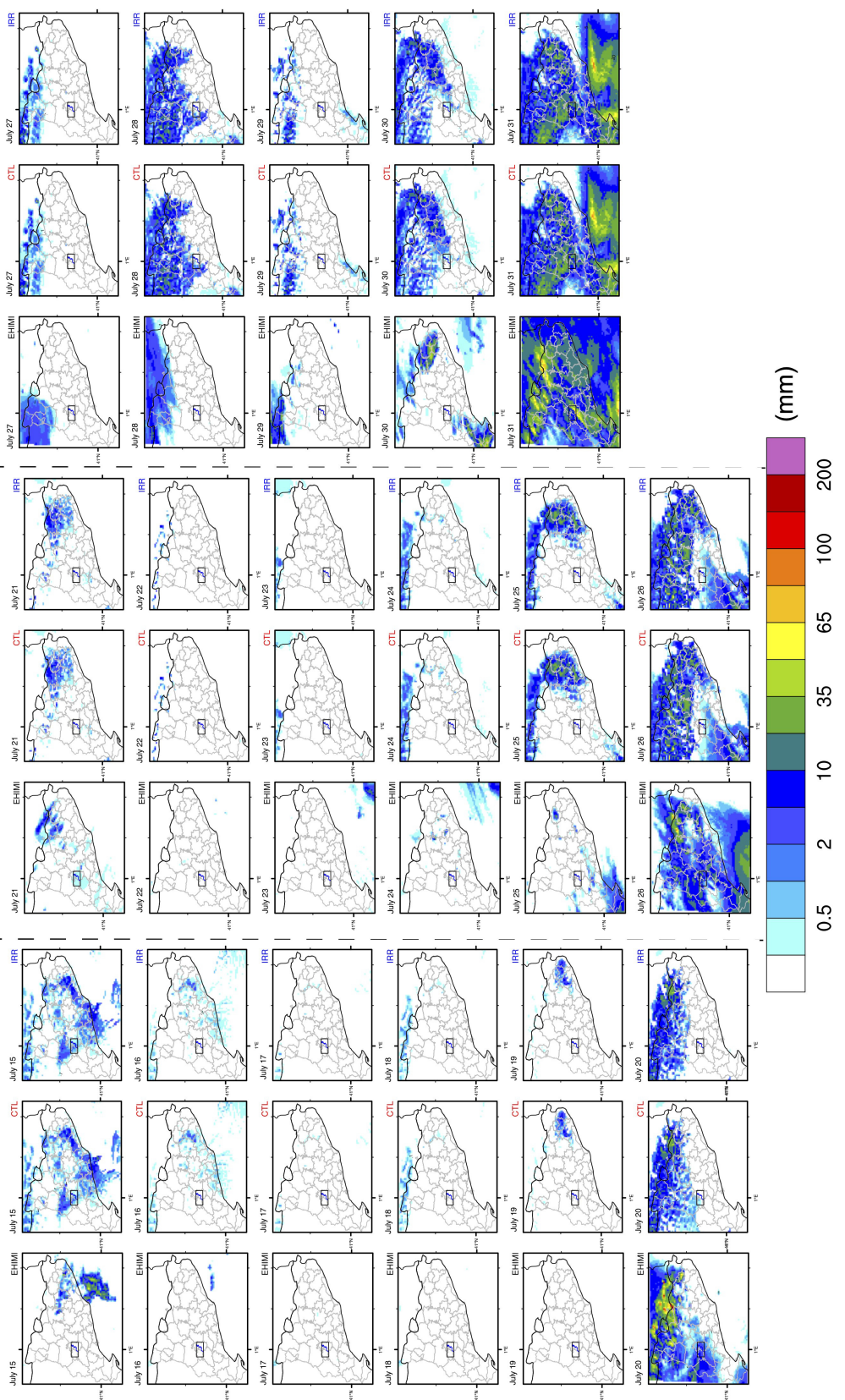


FIGURE C.1 Daily rainfall in Region 0 according to Hydrometeorological Integrated Forecasting Tool (EHIMI) and Weather Research and Forecasting control (CTL) and irrigated (IRR) simulations (convection-parametrized simulations) for the period July 15–31, 2021. The figure is divided (by dashed lines) into three three-column panels, and in each panel the three columns correspond to EHIMI (first column), CTL (second column), and IRR (third column).